SKB

TECHNICAL REPORT 93-31

A preliminary assessment of gas migration from the Copper/Steel Canister

R S Wikramaratna[1], M Goodfield[1], W R Rodwell[1], P J Nash[1], P J Agg[2]

1 AEA Technology, Consultancy Services, Winfrith, UK
2 AEA Technology, Decommissioning & Waste Management, Harwell, UK

November 1993

SVENSK KÄRNBRÄNSLEHANTERING AB
SWEDISH NUCLEAR FUEL AND WASTE MANAGEMENT CO

BOX 5864 S-102 40 STOCKHOLM

TEL. 08-665 28 00 TELEX 13108 SKB S
TELEFAX 08-661 57 19

A PRELIMINARY ASSESSMENT OF GAS MIGRATION FROM THE COPPER/STEEL CANISTER

R S Wikramaratna[1], M Goodfield[1], W R Rodwell[1], P J Nash[1], P J Agg[2]

1 AEA Technology, Consultancy Services, Winfrith, UK
2 AEA Technology, Decommissioning & Waste Management, Harwell, UK

November 1993

A PRELIMINARY ASSESSMENT OF GAS MIGRATION FROM THE COPPER/STEEL CANISTER

R S Wikramaratna†, M Goodfield†, W R Rodwell†,
P J Nash† and P J Agg

† AEA Technology
Consultancy Services
Winfrith

AEA Technology
Decommissioning
& Waste Management
424.4 Harwell
Didcot
Oxfordshire
OX11 0RA

November 1993

A PRELIMINARY ASSESSMENT OF GAS MIGRATION FROM THE COPPER/STEEL CANISTER

R S Wikramaratna, M Goodfield, W R Rodwell,
P J Nash and P J Agg

ABSTRACT

A preliminary assessment has been carried out of the consequences of hydrogen gas generation in the Copper/Steel Canister, a new concept that is being considered by SKB, Sweden, for the encapsulation of spent fuel for geological disposal. The principal aims of the study were as follows:

(a) to determine the mechanisms by which gas generated by anaerobic corrosion will migrate from a canister;
(b) to identify the possible consequences of gas generation, for example overpressurization of the canisters and effects on water movement;
(c) to carry out studies to assess the magnitudes of the consequences of gas generation and the way in which they are influenced by the mechanisms and ease of gas migration;
(d) to determine the likely fate of the gas produced in the repository; for example whether the gas will eventually be dissolved in the groundwater as it moves away from the canister or whether it will collect as free gas in the tunnel or elsewhere;
(e) to identify the potential benefits of using computer modelling techniques for estimating hydrogen generation rates within disposal canisters during the post-emplacement period.

ABSTRACT (Swedish)

En preliminär bedömning har gjorts, av konsekvenserna av gas bildning i koppar-/stålkapseln, ett nytt kapselalternativ som studeras av SKB, för inkapsling av använt kärnbränsle för geologisk förvaring. De huvudsakliga målen för studien var:

(a) bestämma med vilka mekanismer som gas, vilken bildas vid anaerobisk korrosion, transporteras från en kapsel;
(b) identifiera de möjliga konsekvenserna av gasbildning, till exempel trycksättning av kapseln och effekter på grundvattenrörelser;
(c) göra bedömningar av omfattningen av konsekvenserna av gasbildningen och på vilket sätt som de påverkas av gastransportmekanismerna;
(d) att bestämma förloppet för gasen som produceras i ett förvat, till exempel om gasen kommer att lösa sig i grundvattnet eller om den kommer att samlas som fri gas i tunnlarna eller berget;
(e) att bedömma de potentiella fördelarna av att använda datormodellering för att bestämma vätgasproduktionen från kapslarna.

EXECUTIVE SUMMARY

The Copper/Steel Canister is a new concept for the encapsulation of spent nuclear fuel for geological disposal that is being considered by SKB, Sweden. This report describes a preliminary assessment of the consequences of hydrogen gas generation in these disposal canisters.

In the event of water ingress into a canister, hydrogen will be generated as a result of anaerobic corrosion of the carbon steel inner container of the canister. This study has addressed the potential overpressurization of the canister and the possible effects of the gas on water movement around the repository. The principal objectives of this preliminary programme of work were to determine the mechanisms by which gas can migrate from a canister, to identify the possible consequences of gas generation, and to determine the likely fate of the gas produced.

The main conclusions from this preliminary study are as follows:

(a) The long-term effect of hydrogen gas generation will depend on the generation rate and on the ability of the bentonite barrier to permit the escape of the gas.

(b) A number of alternative gas migration routes through the bentonite have been considered, including both the solution of gas in the groundwater and the flow of a gas phase. The amount of gas that could escape through the bentonite by dissolving in the groundwater and diffusing away from the canister is small compared with the maximum gas generation rates that have been considered. Gas-phase flow through the bentonite must therefore represent the primary route for the gas to escape. If the gas generation rate was significantly less than the maximum rate that was assumed in this study, the proportion of gas removed by dissolution and advection in groundwater would be correspondingly greater .

(c) The relationship between the pressure drop across the bentonite and the resulting gas-phase flow rate has been addressed. The scope of this analysis has been limited by the lack of availability of experimental data relating to the mechanisms controlling gas-phase flow through water-saturated bentonite.

(d) Two crucial questions need to be addressed in the future with regard to the passage of gas through the bentonite and the degree of overpressurization of the canister. These questions relate to the numbers (and size) of capillary-like pathways that are present in the bentonite, and the behaviour of the bentonite in response to increasing gas pressure, with respect both to the enlargement of existing pathways and to the formation of new pathways.

(e) Once the gas has escaped from the bentonite, it will pass through into the tunnel area and the damaged zone. Gas-trapping in these zones could cause a small delay in the passage of the gas to the surface; transport of dissolved gas by diffusion or by advection in the groundwater flow is unlikely to represent a significant transport pathway.

(f) The gas will eventually pass into the rock overlying the repository. Two alternative models both suggest that there is ample capacity to transport the gas up towards the surface.

(g) The rate of gas generation is dependent on the availability of water in the canister for metal corrosion to take place. For very small breach sizes the amount of water entering the canister could also be small; future studies should address what effect reduced water ingress might have both on the gas generation rate and also on the potential radiological hazard from H^3H that might arise from contamination of the water with ^3H while it is inside the canister.

CONTENTS

1. INTRODUCTION

The Copper/Steel Canister is a new concept for the encapsulation of spent nuclear fuel for geological disposal that is being considered by SKB of Sweden. This report describes a preliminary assessment of the consequences of hydrogen gas generation in these disposal canisters.

In the event of water ingress into a canister (as a consequence of damage to, defects in or degradation of the canister) hydrogen will be generated as a result of anaerobic corrosion of the carbon steel inner container of the canisters. Such gas production presents something of a dilemma because the primary function of a repository is containment of its contents, whereas if this containment extends to the gas evolved, a build up of pressure will occur, which in time may threaten the integrity of the repository structure or of the surrounding geological environment.

This study has addressed the potential overpressurization of the canisters and the possible effects of the gas on water movement around the disposal facility. The principal objectives of this preliminary programme of work were as follows:

(a) to determine the mechanisms by which gas generated by anaerobic corrosion will migrate from a canister;
(b) to identify the possible consequences of gas generation, for example overpressurization of the canisters and effects on water movement;
(c) to carry out studies to assess the magnitudes of the consequences of gas generation and the way in which they are influenced by the mechanisms and ease of gas migration;
(d) to determine the likely fate of the gas produced in the repository; for example whether the gas will eventually be dissolved in the groundwater as it moves away from the canister or whether it will collect as free gas in the tunnel or elsewhere;
(e) to identify the potential benefits of using computer modelling techniques for estimating hydrogen generation rates within disposal canisters during the post-emplacement period.

The KBS-3 repository design is described in Section 2. The data used in this study are described in Section 3. The studies carried out to address gas migration through the bentonite and through the tunnel and host rock are

described in Sections 4 and 5 respectively. An investigation in the possible implications of gas-water interactions is described in Section 6. A description of the expected long-term fate of the gas is given in Section 7. Finally, the main conclusions of this study are presented in Section 8. In addition, the potential benefits of using computer modelling techniques for estimating hydrogen generation rates (item (e) above) are identified in Appendix A.

2. KBS-3 REPOSITORY DESIGN

2.1 Repository Layout

An overview of the features of the KBS-3 repository layout is given in [1]; the main features are described here. Spent nuclear fuel is encapsulated in copper canisters, which are deposited at a depth in the range 300m to 700m in the bedrock. (In this study, a repository depth of 500m was assumed [2].) The canisters are deposited in holes drilled in the floor of a system of drifts in the rock. The space between canister and rock is filled with bentonite clay. The system of storage drifts is assumed to be regular with a distance of 25m between drifts. The distance between deposition holes is 6m. At closure of the repository, all cavities are backfilled with a sand/bentonite mixture. The drifts are provided with sealing plugs to block potential transport pathways for groundwater.

The number of canisters in a repository is approximately 4000, with the exact layout (length and number of drifts and number of deposition holes per drift) being site dependent [2].

2.2 Canister Design

The basic design of the Copper/Steel Canister [3,4] consists of an outer oxygen-free copper overpack surrounding a carbon steel inner container. The copper overpack is intended to be the principal barrier to corrosion degradation by external groundwater. The main role of the carbon steel container is to provide structural support.

The external dimensions of the canister are approximately 4.5m in length by 0.8m in diameter.

The internal volume of the canister is approximately 1.2 m^3. The fraction of this internal volume taken up by spent fuel is approximately 27%. The

remainder is to be filled with packing materials, leaving a void volume fraction of approximately 35%.

2.2.1 Canister breach

This study has considered the effects of hydrogen gas generation resulting from anaerobic corrosion of the carbon steel inner container following the entry of water into the canister as a result of a breach in the copper overpack. It was assumed that there is a chance of 10^{-3} of such a breach existing in an individual canister at the time of deposition [2]; the initial size of such a breach was assumed to be 5 mm^2 (based on the 2.5 mm diameter of the electron beam used for welding the canisters) and it was assumed to increase in size with time. In the absence of information about growth rates, the size of the breach was treated as a sensitivity parameter and the effects of a range of different breach sizes was assessed. In view of the small probability of an individual canister being breached, this study concentrated on the effects of a breach in a single isolated canister; no attempt was made to consider the consequences of two or more neighbouring canisters being breached.

3. DATA AND DATA SOURCES

Some standard data values used throughout this report are given in Table 1.

3.1 Gas Generation Rates

The intrusion of water or water-saturated bentonite into the canister will result in corrosion of the walls of the carbon steel internal canister. This will result in the production of hydrogen. The gas generation rate and its evolution in time depends on many factors, including the location and size of the breach, the availability of water within the canister, the corrosion rate and the ability of the gas to escape from the canister.

Experimental studies of anaerobic corrosion of carbon steel at temperatures relevant to repository conditions have found the typical corrosion rate to be in the range of 0.2 to 6.5 $\mu m\ yr^{-1}$ [3]. A preliminary assessment of the Copper/Steel Canister [3], in which a number of simplifying assumptions were made, estimated the hydrogen release rates at a pressure of 10 MPa [5] to be in the range between 2 to 6 dm^3yr^{-1}, the exact value depending on the crack location. These rates could persist for 7,000 to 11,000 years. In a more detailed study [6], the initial release rate at 10 MPa was estimated to be

approximately 5 dm^3yr^{-1} for a corrosion rate of 6.5 $\mu m\ yr^{-1}$. In a previous study [4], a worst-case scenario was considered in which the release rate at 10 MPa is 8 dm^3yr^{-1} for the same corrosion rate.

In the present study it was assumed that the hydrogen gas generation rate is constant in time and could range up to the maximum rate of 8 dm^3yr^{-1} at 10 MPa [4] (which corresponds to 0.8 m^3yr^{-1} at atmospheric pressure, 0.1 MPa).

A description of a mathematical model and associated computer program for estimating time-varying gas generation rates in radioactive waste repositories is given in Appendix A. The potential benefits of applying this model to estimating long-term hydrogen gas generation rates in the canisters are also identified.

3.2 Bentonite Properties

The buffer material used to fill the space surrounding each canister in its deposition hole is high-density sodium bentonite clay [1]. The bentonite is not fully saturated at its deposition, so it will take up additional water from the surrounding rock, ultimately becoming saturated. Bentonite clay swells as it takes up water, so if the clay is confined (as it is in the deposition hole) so that swelling is hindered, then a 'swelling pressure' will be exerted on the confining boundaries [7].

The density of the bentonite in the deposition hole can be controlled by taking advantage of its swelling capacity on absorbing water, whereas its permeability can be controlled by varying the smectite content. After water saturation of the repository, the bentonite swelling pressure is expected to reach 10 MPa [5]. The resulting density of the buffer material is around 2.0 $t\ m^{-3}$, and its high smectite content of between 65 to 80% results in a hydraulic conductivity of $10^{-13}\ m\ s^{-1}$ [8].

3.3 Rock Properties

Typical hydraulic conductivities for the repository site have been given based on the 'standard reference case' [8]. The representative value of the hydraulic conductivity for the undisturbed rock was assumed to be $10^{-10}\ m\ s^{-1}$. The drifts (typically 4.5m in diameter) are backfilled with a sand/bentonite mixture having a hydraulic conductivity of $10^{-9}\ m\ s^{-1}$. Surrounding each drift

is a blast-damaged zone approximately 1m thick with a hydraulic conductivity of 10^{-8} m s^{-1}, which is in turn surrounded by a stress-damaged zone some 3.5m thick with a hydraulic conductivity of 10^{-9} m s^{-1}. The individual deposition holes have a diameter of some 1.5m and are surrounded by a damaged zone some 0.05m thick with a hydraulic conductivity of 10^{-9} m s^{-1}. A 'conservative case' has also been described [8], which is similar to the standard reference case described above. However, in this case the blast-damaged zone and the surrounding stress-damaged zone have higher hydraulic conductivities of 10^{-7} m s^{-1} and 10^{-8} m s^{-1} respectively. The hydraulic conductivities of the undisturbed rock and the sand/bentonite mixture are the same as in the standard reference case. A schematic cross section of the tunnel and damaged zones for the conservative case is shown in Figure 1.

In dealing simply with groundwater flow problems it is convenient to work with hydraulic conductivity, which combines properties of both the rock matrix through which the water flows and of the water contained in it. When dealing with multiphase flow problems, such as combined groundwater flow and gas migration, it is more straightforward to work with the permeability, a property of the rock alone. Hydraulic conductivity, K, is measured in m s^{-1} whereas rock permeability, k, is measured in m^2; the relationship between them is

$$K = \frac{k\rho g}{\mu} \quad , \tag{3.1}$$

where ρ is the density and μ the viscosity of water, and g is the acceleration due to gravity. Taking the approximate values $\rho = 10^3$ kg m^{-3}, $\mu = 10^{-3}$ Pa s and $g = 10$ m s^{-2} gives the approximate relationship

$$k = 10^{-7} K \quad . \tag{3.2}$$

Thus, for example, in the case of undisturbed rock given above the permeability is approximately 10^{-17} m^2.

Representative values of the porosities in and around the repository, taken from a number of sources, have been given [9]. The bentonite and sand/bentonite mixture both have a porosity of 25%. The undisturbed rock has a porosity of 0.5%, whereas in the damaged zones the porosity is increased to 1%.

3.4 Regional Groundwater Flow

It is clearly not possible to make any precise statements about regional groundwater flow patterns in the vicinity of the repository without collecting detailed site-specific data. A previous study [8] used a representative value for the regional groundwater head gradient of 0.003 in the direction of the drift.

4. GAS MIGRATION THROUGH BENTONITE

4.1 Diffusion of Gas Dissolved in Groundwater

In this subsection the objective is to estimate the maximum rate at which hydrogen gas could diffuse away from the canister in solution in groundwater. A number of scenarios are considered. In the first case, it was assumed that all the gas would diffuse vertically upwards through the bentonite and be transported away by groundwater flowing through the tunnel backfill. In the second case, it was assumed that the gas would diffuse by the shortest possible route (i.e. radially) to the surrounding rock, where it will be transported away by the groundwater. Note that these first two mechanisms can be assumed to operate independently of one another such that their effects might be additive. A third case was considered in which the gas is assumed to escape from a small breach in the canister and diffuse radially from that point.

The effective diffusivity of dissolved hydrogen (D^*) in compacted bentonite has been discussed in a number of reports; values of $2\ 10^{-11}\ m^2s^{-1}$ [6] and a range of $3.6\ 10^{-12}$ to $1.8\ 10^{-11}\ m^2s^{-1}$ [10] have been reported, based on [11] and [12] respectively. In this study, the higher value of $2\ 10^{-11}\ m^2s^{-1}$ was used as a base case, noting that the lower values were considered to be 'surprisingly low' [11]. The sensitivity of the calculated diffusive fluxes to the value of D^* is discussed in subsection 4.1.4.

The saturation concentration of hydrogen in water can be calculated from Henry's law

$$x = Hp \quad , \tag{4.1.1}$$

where x is the maximum dissolved concentration (m^3(at STP)m^{-3}(solution)), p is the pressure (Pa) and H is the Henry's law coefficient (m^3(at STP)$m^{-3}Pa^{-1}$).

At 20°C the Henry's law Coefficient is around $0.166\ 10^{-6}$ m^3(at STP) $m^{-3}Pa^{-1}$ [13].

The following estimates of diffusive flux assume that the gas pressure does not exceed 15 MPa (the maximum pressure expected, being the sum of the hydrostatic pressure and the swelling pressure of the bentonite), so that the gas concentration will be less than the corresponding saturation concentration of 2.49 m^3m^{-3}.

4.1.1 Case 1: vertical diffusion

This model considers the bentonite above the canister to be in the form of a homogeneous vertical cylinder of radius 0.75m and height 2.75m. A schematic diagram of the model is shown in Figure 2.

The maximum concentration gradient, and hence also the maximum diffusion rate, will exist when the hydrogen concentration is at the saturation concentration just above the canister and falls effectively to zero at the top of the bentonite. This assumes that the groundwater flow across the top of the bentonite removes the dissolved hydrogen sufficiently quickly to maintain the concentration across this surface at effectively zero.

Provided that the pressure does not exceed 15 MPa, the maximum gas diffusive flux can now be calculated from Fick's law

$$Q_g = -D^* \nabla x \quad , \qquad (4.1.2)$$

where Q_g is the gas flux (m^3(at STP)$m^{-2}s^{-1}$), D^* is the effective molecular diffusivity for the dissolved gas in the porous medium (m^2s^{-1}) and x is the dissolved concentration (m^3(at STP)m^{-3}(solution)).

Taking the diffusivity to be $2\ 10^{-11}$ m^2s^{-1} gives a gas flux of approximately $1.81\ 10^{-11}$ m^3(at STP)$m^{-2}s^{-1}$. Based on a cross-sectional area of 1.77 m^2 this gives a gas rate of $1.01\ 10^{-3}$ m^3(at STP)yr^{-1}.

4.1.2 Case 2: radial diffusion

This model considers hydrogen diffusion through the bentonite around the sides of the canister. The external radii of the canister and the bentonite in the deposition hole were assumed to be 0.4m and 0.75m respectively. A schematic diagram of the model is shown in Figure 3.

The hydrogen concentration on the surface of the canister, c_1 was assumed to be the saturation concentration as in the first case (see subsection 4.1.1). The hydrogen concentration at the outer surface of the bentonite, c_2, was assumed to be zero. The gas flux per unit length of the canister can be calculated from the steady-state diffusion equation in radial coordinates (Chapter 7 of [14]), which becomes

$$\frac{d}{dr}\left(r\frac{dx}{dr}\right)=0, \qquad \text{for} \quad a<r<b \ , \tag{4.1.3}$$

assuming no dependence on the radial angle, θ. This equation has the general solution

$$x(r)=A+B\log(r) \ , \tag{4.1.4}$$

where the coefficients A and B are determined from the boundary conditions

$$x(a)=c_1, \quad x(b)=c_2. \tag{4.1.5}$$

Thus

$$x=\frac{c_1\log(b/r)-c_2\log(a/r)}{\log(b)-\log(a)} \ , \tag{4.1.6}$$

and the rate of flow per unit length of cylinder is

$$-2\pi rD^*\frac{dx}{dr}=\frac{2\pi D^*(c_1-c_2)}{\log(b/a)} \ . \tag{4.1.7}$$

Taking the diffusivity to be 2 10^{-11} m^2s^{-1}, this gives a gas rate per unit length of the canister of 1.57 10^{-2} m^3(at STP)$yr^{-1}m^{-1}$. If there is sufficient groundwater flow through the surrounding rock along the entire length of the canister then the gas rate is estimated at 6.91 10^{-2} m^3(at STP)yr^{-1}. However, the damaged zone is only expected to extend about halfway along the canister, which may reduce the gas diffusion rate by up to a factor of two. In either case, this is significantly larger than the estimate obtained for the first case.

4.1.3 Case 3: spherical diffusion

In this case, gas escapes from the canister through a hole, which is assumed to have a radius of 1.25 mm. The gas was assumed to diffuse approximately radially from a point at the centre of the hole. A schematic diagram of the

model is shown in Figure 4. It was further assumed that this can be modelled by steady-state spherical diffusion (Chapter 9 of [14]), the equation for which is

$$\frac{d}{dr}\left(r^2 \frac{dx}{dr}\right) = 0 \ , \tag{4.1.8}$$

assuming that the diffusion depends only on r. This has the general solution

$$x = B + \frac{A}{r} \ . \tag{4.1.9}$$

For a hollow sphere ($a < r < b$) with boundary conditions

$$x(a) = c_1 \quad \text{and} \quad x(b) = c_2 \tag{4.1.10}$$

the solution becomes

$$x(r) = \frac{ac_1(b-r) + bc_2(r-a)}{r(b-a)} \ , \tag{4.1.11}$$

and the rate of flow of gas passing through the hemispherical shell is given by

$$-2\pi r^2 D^* \frac{dx}{dr} = 2\pi D^* \frac{ab}{a-b}(c_2 - c_1) \ . \tag{4.1.12}$$

The approximation of diffusion through a hemispherical shell of bentonite is thought to be conservative since in reality the external boundary will be at least as far away in all directions. Thus, in reality, a lower concentration gradient, and hence also a lower diffusion rate, would be expected.

It was assumed that the gas concentration at the inside of the hemisphere would be the saturation concentration and that the gas concentration at the external surface would be zero. The same value of the gas diffusivity was used as in the first and second cases (see subsections 4.1.1 and 4.1.2 respectively). Taking the internal and external radii to be 1.25 10^{-3}m and 0.35m respectively, this gives a diffusion rate of 1.24 10^{-5} m^3(at STP)yr^{-1}. It should be noted that an increase in the size of the hole (and hence in the inner radius, a) will lead to an approximately proportional increase in the diffusion rate as long as a remains significantly less than b. Increasing the radius of the hole to 12.5 mm would thus result in a diffusion rate of 1.24 10^{-4} m^3(at STP)yr^{-1}. As would be expected intuitively, the calculated

spherical diffusion rate is significantly less than the radial diffusion rate calculated (see subsection 4.1.2).

4.1.4 Estimate of total diffusive flux

An upper bound on the total potential diffusive flux is obtained by combining the estimates from the first and second cases (see subsections 4.1.1 and 4.1.2). The resulting flux of 7.01 10^{-2} m^3(at STP)yr^{-1} is dominated by the radial component and is at least one order of magnitude lower than the maximum gas generation rate of 0.8 m^3(at STP)yr^{-1}. The estimate is based on a diffusion coefficient at the maximum of the reported range and on the assumption that the gas will spread out over the entire vertical external surface of the canister at a pressure of 15 MPa, that the hydrogen will dissolve in the water up to the saturation concentration over this surface, and that the groundwater flow in the damaged zone is sufficient to maintain the gas concentration along this boundary effectively at zero. If any of these assumptions are not met then the actual diffusion rate could be considerably lower. For example, spherical diffusion from a small hole (radius up to 12.5 mm diameter) is at least three orders of magnitude lower than the maximum gas generation rate, and any reduction in the diffusion coefficient would lead to a proportional reduction in the calculated flux for each of the three cases considered.

4.2 Gas-Phase Flow through Bentonite

A previous experimental study [15] was primarily aimed at testing the hypothesis of the 'critical pressure concept' for gas-phase flow through saturated bentonite. This hypothesis is that there is a minimum pressure below which gas-phase flow cannot occur; once this pressure is exceeded, gas-phase flow can commence. The experiments involved the measurement of the gas flow as a function of the applied, successively increased gas pressure, together with an attempt to identify microstructural evidence for how gas percolates through clay. It was concluded that, in soft and medium-dense bentonite, capillary pressure probably provides the major resistance to gas propagation, whereas in dense bentonite the penetrating gas has to make its way by displacing clay aggregates. In the latter case the critical pressure is argued to be high and close to the swelling pressure. It has been found empirically that the critical pressure is 50 to 90% of the swelling pressure [16].

A mathematical model is described in subsections 4.2.1 to 4.2.3 for flow in capillary-like pathways that already exist in the bentonite. For any given gas flow rate, the pressure rise that results will depend on the number of capillaries that are present in the bentonite. If the estimated pressure rise is sufficient, it may be necessary to consider displacement of clay aggregates to enlarge existing capillaries or to form new ones.

4.2.1 Estimation of capillary pressures

The average capillary diameter of highly saturated, highly compacted and matured bentonite is estimated to be about 5 10^{-8}m [17] with 90th and 10th percentiles of 10^{-6}m and 5 10^{-9}m respectively. The capillary pressure, p_c, at the gas-water interface can be estimated from the expression

$$p_c = \frac{2\sigma}{r} \quad . \tag{4.2.1}$$

Here, σ is the surface tension of the water and r is the radius of the capillary. Taking the surface tension to be 0.073 Nm^{-1} (see Table 1), this gives a capillary pressure of 5.84 MPa for the average capillary diameter. Similarly, capillary pressures of 0.292 MPa and 58.4 MPa are obtained for the 90th and 10th percentile radii respectively.

4.2.2 Single-capillary model

If the gas flow is controlled solely by capillary retention then a simple model can be derived for the flow through bentonite. Gas flow is assumed to be along uniform horizontal capillaries extending radially from the canister out through the bentonite to the surrounding rock. A single capillary is considered of radius r and length L. It is also assumed that the pressure in the canister is sufficiently high for the gas to have reached the surrounding rock. The gas flow then satisfies the conservation equation and Darcy's equation:

$$\frac{\partial \rho_g}{\partial t} + \frac{\partial}{\partial x}(\rho_g u_g) = 0 \qquad \text{and} \qquad u_g = -\frac{k}{\mu_g}\frac{\partial p_g}{\partial x} \quad , \tag{4.2.2}$$

where ρ_g is the gas density, u_g is the Darcy flux of the gas, p_g is the gas pressure, k is the permeability of the capillary, μ_g is the gas viscosity, x is the horizontal displacement and t is the time. If it is further assumed that the

gas is effectively incompressible then the conservation equation and Darcy's equation yield

$$\frac{\partial^2 p_g}{\partial x^2} = 0 \quad , \tag{4.2.3}$$

which has a solution of the form

$$p_g = Ax + B \quad . \tag{4.2.4}$$

For the boundary conditions $p_g = p_A$ at $x = 0$ and $p_g = p_B$ at $x = L$, this becomes

$$p_g = \frac{(p_B - p_A)}{L} x + p_A \quad . \tag{4.2.5}$$

Taking the permeability of the capillary to be $k = r^2/8$ [13] and substituting the above expression into Darcy's equation gives

$$u_g = \frac{r^2}{8\mu_g} \frac{(p_A - p_B)}{L} \quad . \tag{4.2.6}$$

If the pressure at the internal face of the bentonite is lower than the sum of the pressure at the external face and the capillary pressure, p_c, there will be no flow. Thus the gas flow rate in the capillary, q_g, for a given pressure drop, p_A–p_B, is given by

$$q_g = \begin{cases} \dfrac{\pi r^4}{8\mu_g} \dfrac{(p_A - p_B)}{L}, & p_A - p_B > p_c \\ 0, & p_A - p_B \le p_c \end{cases} \quad . \tag{4.2.7}$$

This gives an expression for steady-state gas-phase flow in a capillary, ignoring the transient period during which the water is flushed from the capillary. It is assumed that capillary pressure no longer retards the gas flow once the water has been swept from the capillary. This is only true if the capillary pressure of the rock adjacent to the external surface of the bentonite is negligible.

4.2.3 Model for a distribution of capillaries

If instead of a single capillary, the bentonite contains a number of capillaries with a specified distribution of radii then the total flow rate will be the sum of the flow rates from each of the individual capillaries. If $f(r)$ is the probability

density function for the capillary radius then the normalized total flow rate, Q, can be written as

$$Q = \frac{q_T}{N_c} = \int_0^\infty q_g(r) f(r) dr \quad , \tag{4.2.8}$$

where q_T is the total flow rate and N_c is the number of capillaries. The capillary flow rate in a particular capillary is zero when the pressure difference is less than the capillary pressure. That is, the flow rate is zero when

$$p_A - p_B \le p_c = \frac{2\sigma}{r}, \quad \text{or} \quad r \le \frac{2\sigma}{p_A - p_B} = r_0 \quad , \tag{4.2.9}$$

taking into account equation (4.2.1).

The normalized total flow rate (equation (4.2.8)) can then be expressed as

$$Q = \int_{r_0}^\infty q_g(r) f(r) dr = \frac{\pi}{8\mu_g} \frac{\Delta p}{L} \int_{r_0}^\infty r^4 f(r) dr \quad , \tag{4.2.10}$$

where $\Delta p = p_A - p_B$. Now if the radii have a log-normal distribution with parameters (μ_R , σ_R), so that log(r) has a normal distribution with mean μ_R and standard deviation σ_R, then

$$f(r) = \frac{1}{r\sigma_R\sqrt{2\pi}} \exp\left\{-\frac{1}{2}\left(\frac{\log r - \mu_R}{\sigma_R}\right)^2\right\} \tag{4.2.11}$$

Substituting this into equation (4.2.10) and integrating gives

$$Q = \frac{\pi \Delta p \exp[4(\mu_R + 2\sigma_R^2)]}{16\mu_g L} \operatorname{erfc}\left(\frac{\log r_0 - \mu_R - 4\sigma_R^2}{\sqrt{2}\sigma_R}\right) \tag{4.2.12}$$

The gas flow rate can thus be obtained for a given pressure drop. Note that in reality each capillary will have a variable radius along its length and the capillary retention will be dependent on the minimum radius of the capillary.

4.2.4 Results

A horizontal capillary was considered, extending radially from the canister to the surrounding rock, so that it has a length of 0.35m. It was assumed that the pressure drop across the bentonite is equal to the critical pressure (taken here to be 60% of the swelling pressure or 6 MPa), and that the pressure at

the external surface of the bentonite is equal to the hydrostatic pressure at the repository depth. It was also assumed that the capillary has uniform radius equal to the average capillary radius of 2.5 10^{-8}m (see subsection 4.2.1). Taking the gas viscosity to be 10^{-5} Pa s in equation (4.2.7), this gives a gas rate in the capillary of 2.10 10^{-17} m^3(at STP)s^{-1} or 6.64 10^{-10} m^3(at STP)yr^{-1}. At the maximum gas generation rate of 0.8 m^3(at STP)yr^{-1} (see subsection 3.1), approximately 1.21 10^9 such capillaries would be required to support flow with this pressure drop.

The capillaries being considered are horizontal and extend radially through the bentonite annulus which was assumed to have a height of 4.5m, an internal radius of 0.4m and an external radius of 0.75m. The area of the bentonite perpendicular to the flow is therefore in the range 11.3 to 21.2 m^2. In order to support gas flow at the maximum gas generation rate, the density of such capillaries would therefore need to be in the range 5.69 10^7 to 1.07 10^8 m^{-2}. A value of 10^8 m^{-2}, corresponds to capillaries being spaced at intervals of 10^{-4}m if they are arranged in a uniform square array. If the gas flow were to be confined to a fraction of the bentonite annulus (e.g. the region of the annulus in the immediate vicinity of a small breach) then the density of capillaries required would be correspondingly higher. If the gas generation rate were significantly lower than the maximum rate assumed in these calculations, the density of capillaries required to support gas flow would clearly be correspondingly lower.

4.2.5 Displacement of clay aggregates

In the previous subsections, calculations have been performed that relate the pressure rise in the canister to the gas generation rate and the number and size distribution of capillary-like pathways already existing in the bentonite. As long as the pressure rise in the bentonite is not too large, the assumption that the gas flow will occur solely in pre-existing pathways is reasonable. However, if the pressure rises sufficiently (certainly once the gas pressure begins to approach the sum of the swelling pressure and the hydrostatic pressure at the repository depth), deformation of the bentonite may occur, either enlarging existing pathways or creating new ones. The effects of any such deformation would be greatest in the immediate vicinity of the canister, where the pressure is highest, and would diminish with increasing distance from it. In terms of the flow capacity of the bentonite, such deformation

would tend to increase the gas flow for a given pressure drop, as compared with the calculations that assume no deformation.

An understanding of the mechanisms controlling the displacement of clay aggregates is important in assessing the potential overpressurization of the canister. However, it is beyond the scope of this work to attempt to model these effects. Also, the long-term effects of gas migration on the properties of bentonite are outside the scope of this report and may need to be addressed in the future.

5. GAS MIGRATION IN TUNNEL AND HOST ROCK

5.1 Transport of Dissolved Gas by Groundwater Advection

5.1.1 Advection in the tunnel and damaged zones

The gas may dissolve and be carried away by advection in the groundwater flowing through the tunnel backfill and damaged zone in the direction of the drift. In order to estimate the maximum rate at which dissolved gas can be advected away by the groundwater it was assumed that gas spreads out across the entire cross-sectional area of the tunnel and the damaged zone. The advection rate is simply estimated as the product of the saturation concentration of hydrogen gas in water, x, and the water flow rate integrated over the cross-sectional area of the tunnel. The pressure was assumed to be constant over this area.

The saturation concentration of hydrogen in water can be calculated from Henry's law (equation (4.1.1)). The pressure was assumed to be the hydrostatic pressure of approximately 5 MPa (see Table 1). The regional hydraulic gradient was assumed to be 0.003 (see subsection 3.4), which is equivalent to a regional pressure gradient of approximately 30 Pa m^{-1}. The advection rate of dissolved gas, q (m^3(at STP)s^{-1}), across an area, A, is given by

$$q = Hpu_w A \quad , \tag{5.1.1}$$

in which u_w is the water flux (m s^{-1}), which can be obtained from Darcy's equation

$$u_w = -\frac{k}{\mu_w}\nabla p \quad , \tag{5.1.2}$$

where k is the permeability (m^2), ∇p is the regional pressure gradient (Pa m^{-1}) and μ_w is the water viscosity (Pa s).

The cross section of the tunnel and the rock properties associated with each of the zones are illustrated in Figure 1 and were discussed in subsection 3.3. The higher hydraulic conductivities of the blast- and stress-damaged zones in the conservative case were used to estimate the maximum rate of advection of dissolved gas. The area, water flux and maximum rate of advection of dissolved gas for each zone are given in Table 2. The low permeability of the tunnel backfill leads to a very low rate of advection of dissolved gas. The area of the blast-damaged zone is similar to that of the tunnel, but the higher permeability results in a corresponding higher advection rate (by two orders of magnitude). The stress-damaged zone has a significantly larger area, although this is counteracted by a lower permeability, so that the advection rate here is an order of magnitude less than in the blast-damaged zone.

The maximum total advection rate for dissolved gas represents a significant proportion (approximately 25%) when compared with the maximum gas generation rate of 0.8 m^3(at STP)yr^{-1} (see subsection 3.1). A similar analysis in which the hydraulic conductivities are taken from the standard reference case (see subsection 3.3) gives a total advection rate for dissolved gas a factor of ten times lower than that for the conservative case. However, both these analyses could be greatly overestimating the rate by assuming that the gas spreads out across the entire cross section of the tunnel and damaged zones, and that it is dissolved up to the saturation concentration throughout. In practice, therefore, it is expected that advection in the tunnel and damaged zones would only be sufficient to remove a small proportion of the generated gas. If the gas generation rate were significantly less than the maximum rate assumed in this study, the proportion of gas removed by advection would clearly be correspondingly greater .

5.1.2 Advection in a network of channels

A model has previously been considered for flow in fractures [8] that assumed the existence of three virtually orthogonal sets of fracture planes (two vertical and one horizontal). An important feature of that model is that the fractures do not act as plane parallel slots, but allow fluids to flow in channels located along the intersections between pairs of fracture planes. As far as the flows

are concerned, the system can be considered as three orthogonal sets of intersecting channels.

If the gas is not completely dissolved in the groundwater flowing in the tunnel and damaged zones then it may enter a fracture channel in the host rock and flow upwards to the surface under the influence of buoyancy forces and pressure gradients. During this time some or all of this remaining gas could be dissolved in the groundwater flowing in horizontal channels that intersect the pathway to the surface.

5.1.3 Discrete model for advection from channels

To estimate the volume of gas that could be dissolved and advected away by the groundwater, several simplifying assumptions have been made to the model described in subsection 5.1.2. It was assumed that the gas travels directly to the surface along a single channel at the intersection between two vertical fracture planes. It is further assumed that the regional pressure gradient is parallel to one of these fracture planes (and normal to the other), so that all the water flow will be confined to a single vertical fracture plane.

The model therefore consists of a single vertical gas channel with water flowing in a number of horizontal channels intersecting the vertical channel at regular intervals along its length. This is illustrated schematically in Figure 5; note that it is assumed that the gas and water flows intermingle at the intersections, and that all the water contacting gas at the intersections between channels becomes fully saturated with gas. These assumptions lead to an upper bound on the volume of gas that could be dissolved and advected away by the groundwater.

The channels consist of fourth-order discontinuities (defined in a previous study [8]), which represent the hydraulically active members of the host rock, with an aperture, a, of 100 μm, a width, w, of 1 cm and a spacing, l, of 5m [8]. The bulk hydraulic conductivity calculated for rock containing just fourth-order discontinuities is consistent, to within a factor of four, with the overall value of 10^{-17} m^2 for the rock given in [8]. Since the fracture apertures, widths and spacings and the overall value for the hydraulic conductivity are all quoted to just one significant figure, this agreement is as good as can be expected. The regional hydraulic gradient was assumed to be 0.003 (see subsection 3.4), which is equivalent to a regional pressure gradient of around 30 Pa m^{-1}.

The saturation concentration of hydrogen in water can be calculated from Henry's law (equation (4.1.1)). The pressure, p (Pa), is taken as the hydrostatic pressure

$$p = p_0 + \rho_w g z \quad , \tag{5.1.3}$$

where ρ_w is the water density (kg m^{-3}), p_0 is the surface pressure (Pa) and z is the depth below the surface (m). Considering equation (5.1.1), the rate (m^3(at STP)s^{-1}) at which gas could be dissolved and removed by advection in the groundwater flowing across an intersection is

$$q = Hpu_w aw \quad , \tag{5.1.4}$$

where u_w is the water flux (m s^{-1}), which can be obtained from Darcy's equation (5.1.2), in which the channel permeability, $k = a^2/12$ (m^2). If the horizontal channels are evenly spaced at a distance l (m) and the vertical channel has a total height of d (m), there will be a total of $N = \text{int}(d/l + \frac{1}{2})$ horizontal channels, which are assumed to be at depths

$$z = d - (n - \tfrac{1}{2})l, \text{ for } n = 1, \cdots N \quad . \tag{5.1.5}$$

The advection rate from M intersections up from the repository (m^3(at STP)s^{-1}), q_M, is simply the sum of the rates from each of the intersections

$$q_M = Hu_w aw \sum_{n=1}^{M} \{p_0 + \rho_w g(d - (n - \tfrac{1}{2})l)\} \quad , \tag{5.1.6}$$

which becomes

$$q_M = Hu_w aw\rho_w g \left\{ M\left(\frac{p_0}{\rho_w g} + d \right) - \tfrac{1}{2} M^2 l \right\} \quad . \tag{5.1.7}$$

The number of intersections required before all the gas is removed can be estimated by equating the advection rate, q_M to the gas generation rate, q_g. This gives a quadratic equation for M,

$$\tfrac{1}{2} M^2 l - \left(\frac{p_0}{\rho_w g} + d \right) M + \frac{q_g}{Hu_w aw\rho_w g} = 0 \quad , \tag{5.1.8}$$

which has two solutions. The solution that gives the correct limiting behaviour as the gas generation rate tends to zero is

$$M = \frac{1}{l}\left\{(\alpha + d) - \sqrt{(\alpha + d)^2 - \beta \frac{q_g}{u_w a \lambda}}\right\} \qquad (5.1.9)$$

in which $\alpha = \frac{p_0}{\rho_w g}$, $\beta = \frac{2}{H \rho_w g}$ and $\lambda = \frac{w}{l}$. If the term within the square root sign is negative, then there will not be a real solution for M. This will occur when the total groundwater flow, summed over the depth d, is insufficient to dissolve all of the gas, in which case gas will be able to reach the surface. Conversely, if the term within the square root sign is positive, then the groundwater flow can potentially dissolve all of the gas. The depth at which all the gas will have been dissolved can then be determined from the solution of equation (5.1.8).

Substituting the data given in Table 1 into equation (5.1.9) indicates that not all of the generated gas will be dissolved in the groundwater. The dissolved gas could be advected away by the groundwater at a rate of no more than $3.25\ 10^{-2}$ m^3(at STP)yr^{-1} which is greater than one order of magnitude lower than the maximum gas generation rate.

5.2 Gas-Trapping in the Tunnel Area

The passage of gas to the far field may be delayed by trapping in the tunnel backfill or in the damaged zones. The following analysis looks at the possible significance of such trapping in delaying the passage of gas.

In a previous study [18], consideration was given to the capillary pressure conditions that are necessary for the accumulation of gas at the boundary interface between two rock zones with different physical properties. The significant conclusions were that the capillary pressure in the overlying rock zone needs to be higher than that in the lower zone, and that the thickness of the cushion of trapped gas that may accumulate is then dependent on the difference in the capillary pressure between the zones.

In the analysis that follows, estimates are obtained of the volumes of gas that may become trapped at the interface between the tunnel backfill and the blast-damaged zone, and at the upper boundaries of the blast- and stress-damaged zones. In each case, the capillary pressures are overestimated for the overlying zone and underestimated (set to zero) for the lower zone. This conservatism ensures that the estimate provides an upper bound on the true potential for gas-trapping.

In practice, the volume of trapped gas per unit length of tunnel may be considerably less than the estimate, owing to two facts. First, a significant proportion of the water present in the sand/bentonite mixture may be trapped and unable to be displaced by the gas [19]. Secondly, the capillary pressure in the sand/bentonite mixture is expected to be significant and may even exceed that in the blast-damaged zone; in the latter case there will clearly be no trapping of gas at this interface.

5.2.1 Gas storage in the tunnel

The pore volume of the tunnel per metre length of tunnel is the product of the porosity and the cross-sectional area. The tunnel was assumed to have a diameter of 4.5m and a porosity, ϕ, of 25% (see Figure 1), so that the pore volume per unit length is 3.98 m^3m^{-1}.

It was assumed that gas can become trapped at the interfaces between the tunnel backfill and the blast-damaged zone. This may only be the case if there is initially no continuity of the capillary pressures between these zones. If this is the case the gas will remain trapped until the excess pressure in the gas volume becomes greater than the capillary pressure of the largest channel in contact with the gas.

Since the pressure drop across the height of the gas volume will be small, the excess pressure of the gas will be roughly equal to a hydrostatic head of the same height. The excess pressure is thus given by

$$p = \rho_w g h \quad , \tag{5.2.1}$$

where ρ_w is the water density (kg m^{-3}), g is the acceleration due to gravity (m s^{-2}) and h is the height of the gas volume (m). If the gas volume is in contact with a fracture channel with aperture, a, then the capillary pressure, p_c, (Pa) of the channel [13] is given by

$$p_c = \frac{2\sigma}{a} \quad , \tag{5.2.2}$$

where σ is the surface tension of water (0.073 N m^{-1}, see Table 1). The gas will begin to enter the channel when the excess pressure equals the capillary pressure. The height of the gas volume as this happens can be obtained by combining equations (5.2.1) and (5.2.2). It was assumed that the tunnel has a

circular cross section that extends horizontally along the length of the tunnel. The volume of gas trapped per unit length of tunnel (m^3m^{-1}) is then given by

$$V = r^2(\theta - \sin\theta\cos\theta)\phi \quad , \tag{5.2.3}$$

in which

$$\theta = \cos^{-1}\left(\frac{r-h}{r}\right) \quad , \tag{5.2.4}$$

where r is the radius of the tunnel (m), and ϕ is the porosity of the tunnel. It was assumed that the only channels in the rock are fourth-order discontinuities so that the capillary pressure of the channels is 1.46 10^3 Pa (see subsection 5.1.3 and equation (5.2.2)). Therefore, following the above analysis, an upper bound on the height of the gas volume will be 0.149m. This gives a volume per unit length of 4.07 10^{-2} m^3m^{-1}, which is equivalent to a gas volume of 2.03 m^3(at STP)m^{-1}.

5.2.2 Gas storage in damaged zones

It is possible to apply the same analysis as in subsection 5.2.1 to show that the trapped gas volume per unit length in the blast- and stress-damaged zones will not be more than 0.098 m^3(at STP)m^{-1} and 0.142 m^3(at STP)m^{-1} respectively. Thus the volume of gas trapped in the damaged zone will be at least one order of magnitude less than the upper bound on the volume that may become trapped in the tunnel.

5.2.3 Effects of gas-trapping

In practice there is expected to be a fourth-order fracture on average every 5m along the length of the tunnel [8]. A reasonable estimate of the volume of gas that may become trapped in the tunnel can be obtained by assuming a gas volume of height 0.149m extending over the section of tunnel between two fourth-order fractures. It is of course possible that the gas will spread out in a thinner layer over a larger length of the tunnel, so that the capillary pressure of the fourth-order fractures is not overcome. However, it seems likely that the requirement of even a 0.149m thickness is likely to be unnecessary because, first, the effects of constructing the tunnel are likely to have enlarged the fractures close to the boundary between the damaged zone and the tunnel, and secondly, any unevenness in the tunnel surface is likely to inhibit the horizontal movement of the gas, causing it to accumulate close

to the source rather than spreading in a very thin layer along the top of the tunnel.

The resulting upper bound of 11.35 m^3(at STP) of trapped gas represents some 14.4 years of gas production. The effects of gas-trapping are therefore unlikely to delay the passage of gas into the fracture system by more than this period.

5.3 Gas-Phase Transport in the Fracture System

Assuming that the gas behaves ideally and travels vertically up through established pathways in the rock, the gas flux, Q_g, can be estimated from Darcy's law [13]

$$Q_g = \frac{k^*(p_r^2 - p_s^2)}{2\mu_g p_0 d} \quad , \tag{5.3.1}$$

where, k^* is the effective rock permeability (m^2), p_r and p_s are the repository and surface pressures respectively (Pa), p_0 is the standard pressure used in specifying the gas flux (Pa), μ_g is the gas viscosity (Pa s), and d is the repository depth (m).

5.3.1 Continuum model

For a given gas flux equation (5.3.1) can be rearranged to estimate the effective permeability needed to allow the gas to escape once steady-state pathways have been established. Suppose that the surface and the standard pressure are both taken to be 0.1 MPa, the repository depth is 500m, the repository pressure is equal to the hydrostatic head (5 MPa) and the gas viscosity is 10^{-5} Pa s (see Table 1). Then if the gas spreads out over an area of 1 m^2 the required effective permeability will be 10^{-18} m^2 for the maximum initial gas generation rate of 0.8 m^3(at STP)yr^{-1} (see subsection 3.1). If the gas spreads out to an area of 100 m^2 then the required effective permeability will be 10^{-20} m^2. If these effective permeability values are compared with the actual value of 10^{-17} m^2 for undisturbed rock, it is clear that the gas should have little difficulty in escaping to the surface once a pathway has been established.

5.3.2 Discrete-fracture model

An alternative approach is to consider the flow rate in individual fractures. The repository was assumed to be linked to the surface by a single series of interconnecting channels within fourth-order discontinuities. The possible gas flow rate, once a steady-state pathway has been established, can then be estimated from Darcy's law (equation 5.3.1). If L is the actual length of the pathway, then L/d is a measure of its tortuosity, where d is the repository depth. If the actual pathway is approximated by a straight channel inclined at an angle $\cos^{-1}(d/L)$ to the vertical, the gas flux can be estimated from an expression analogous to equation (5.3.1):

$$Q_g = \frac{k^*(p_r^2 - p_s^2)}{2\mu_g p_o L} \quad . \tag{5.3.2}$$

The effective permeability of a fracture of aperture, a, is given as [13]

$$k^* = \frac{a^2}{12} \quad . \tag{5.3.3}$$

If the pathway has dimensions as described in subsection 5.1.3 then the gas rate is estimated to be 660 m^3(at STP)yr^{-1} and 330 m^3(at STP)yr^{-1} for $L = d$ and $L = 2d$ respectively. This is two to three orders of magnitude higher than the maximum initial gas generation rate. Thus provided the gas can escape from the canister and the bentonite, it will be able to reach the surface fairly easily once a pathway between the repository and the surface has been established.

It is useful to consider the volume of gas required to fill such a channel. If the channel has a uniform cross-sectional area, A, then the volume of gas at surface pressure required to fill the channel is given by

$$V_g = \frac{AL}{p_0}\left(\frac{p_s + p_r}{2}\right) \quad . \tag{5.3.4}$$

Assuming the pathway to have dimensions as described in subsection 5.1.3, the volume of gas (at STP) required to fill the channel is estimated to be 0.0128 m^3 and 0.0255 m^3 for $L = d$ and $L = 2d$ respectively.

Once a pathway has been established storage of gas within the channel is unlikely to be a significant factor; however it is still relevant to consider the timescale over which such pathways might become established.

6. GAS-WATER INTERACTIONS

At the time of disposal, the canister is likely to contain dry gas at atmospheric pressure. Following breach of the canister, water will flow into the canister and hydrogen gas will be generated by anaerobic metal corrosion. The gas pressure will rise as a result of both the gas generation and the water intrusion until the pressure inside the canister becomes equal to the hydrostatic pressure at the repository depth. The flow will then reverse until the water level in the canister falls below the breach; from this time onwards the flow will cease until the pressure has risen sufficiently for gas-phase flow in the bentonite to commence.

The model described above for the flows of water into and out of the canister following a breach is essentially the same as that proposed in a previous study [20] and subsequently used to investigate gas-water interactions [4].

In the previous study [20], the entire problem was solved numerically using a finite-element solution method. The flow problem was solved assuming that the water was compressible so that the transient effects of changes to the flow field were included in the model.

In the subsequent investigation [4], the flow through the bentonite was treated by assuming that the water was incompressible so that changes to the flow field occurred instantaneously when the boundary pressures in the bentonite changed. This allowed the flow rate to be related to the instantaneous pressure differences across the bentonite; the resulting ordinary differential equation for the volume of water in the canister and the corresponding pressure was obtained by solving the equation numerically.

The results presented in the two previous studies [20,4] were concerned mainly with the case of a cylindrical crack in the canister surface. In this study, the main concern is with the consequences of a small hole at one point in the canister. The mathematical analysis of this problem is considered in the following subsections.

6.1 Mathematical Analysis of Flow into the Canister

Consider a hemispherical shell of bentonite with internal radius a and external radius b. In this model a represents the radius of the breach, and b

represents the thickness of the bentonite. Suppose the pressure is $p = p_a$ at $r = a$ and $p = p_b$ at $r = b$. The Darcy flux is

$$q = -\frac{k}{\mu}\nabla p \ , \qquad (6.1.1)$$

where k is the permeability (m^2) of the bentonite, μ is the water viscosity and p is the pressure. The assumption of spherical flow towards the breach leads to an equation for the pressure of the same form as equation (4.1.11) for the gas concentration, and an equation similar to equation (4.1.12) for Q, the rate of flow of water through the hemispherical shell:

$$Q = -2\pi r^2 \frac{k}{\mu}\nabla p = -2\pi \frac{k}{\mu}\frac{ab}{(b-a)}(p_b - p_a) = -K_1^*(p_b - p_a) \ , \qquad (6.1.2)$$

where the constant $K_1{}^*$ is defined by this equation. This gives a simple relationship between the flow rate and the pressure drop across the bentonite. Note that provided the internal radius is much smaller than the external radius ($a << b$) the precise value chosen for b is of little significance as long as p_b remains fixed. It is therefore reasonable to take b equal to the thickness of the bentonite and set p_b to be equal to the hydrostatic pressure at the repository depth.

The analysis above applies to the case where the position of the breach is well away from the edges of the canister (either near the middle of the bottom face or some way up the side of the canister). If the breach lies on the edge, then the appropriate model is likely to be a bentonite shell forming three quarters of a sphere rather than a hemisphere, such that the value of $K_1{}^*$ should be increased by a factor of 1.5; if the breach lies close to but not on the edge, then an intermediate value may be more appropriate.

In solving for the flows and pressure, two distinct periods need to be considered: the period of water flow into and out of the hole; and the period of no flow once the water level in the canister has fallen to the level of the hole. These two periods are discussed in subsections 6.1.1 and 6.1.2 respectively.

6.1.1 Water inflow/outflow period

If the void volume of the canister is V_v (equal to the internal volume of the canister, less the volume of the waste and packing material), then the initial gas content of the canister will be V_v at atmospheric pressure, p_0. If the gas

generation rate measured at p_0 is g_0, assumed constant, and if $V_g(t)$ is the volume of gas in the canister at time t, then

$$\frac{dV_g}{dt} = -K_1^*(p_b - p_a) \ , \tag{6.1.3}$$

where p_b is constant and p_a is given by

$$p_a(t) = \left(\frac{V_v + tg_o}{V_g(t)}\right)p_o \ , \tag{6.1.4}$$

and where the initial condition is $V_g = V_v$ at $t = 0$. The differential equation (6.1.3) can be solved as follows. Making the following substitutions,

$$\left.\begin{array}{lll} \alpha = K_1^* p_b & \beta = K_1^* V_v p_o & \gamma = K_1^* g_o p_o \\ \theta_1 = \alpha/\gamma & \theta_2 = 1/\gamma & x = \beta + \gamma t \end{array}\right\} \ , \tag{6.1.5}$$

the equation (6.1.3) can be written in the form

$$\frac{dV_g}{dx} = -\theta_1 + \theta_2 \frac{x}{V_g} = f\left(V_g/x\right) \ , \tag{6.1.6}$$

where

$$f(z) = -\theta_1 + \theta_2/z \ . \tag{6.1.7}$$

Writing $z = V_g/x$ leads to a separable equation of the form

$$\frac{dx}{x} = \frac{-zdz}{z^2 + \theta_1 z - \theta_2} \ , \tag{6.1.8}$$

for which the solution is given by

$$\log\left|V_g^2 + \theta_1 x V_g - \theta_2 x^2\right| - \frac{\theta_1}{\left(\theta_1^2 + 4\theta_2\right)^{1/2}} \log\left|\frac{2V_g + x\theta_1 - x\left(\theta_1^2 + 4\theta_2\right)^{1/2}}{2V_g + x\theta_1 + x\left(\theta_1^2 + 4\theta_2\right)^{1/2}}\right| + C = 0 \ . \tag{6.1.9}$$

This equation can be solved in a straightforward manner to give V_g at any time, by the following procedure:

(i) put $t = 0$ (i.e. $x = \beta$) and $V_g = V_v$ in equation (6.1.9) and evaluate the constant, C;

(ii) at any given time $t > 0$, put $x = \beta + \gamma t$ and the value of C determined in (i) into equation (6.1.9), and solve the resulting equation for V_g (e.g. by

using Newton iteration). The volume of water in the canister is given simply by $V_w = V_v - V_g$;

(iii) evaluate the pressure in the canister using equation (6.1.4).

6.1.2 Period of pressure increase (no flow)

Once the water level in the canister has fallen to the level of the hole, the water will no longer flow out, but the pressure will continue to increase until there is sufficient pressure for gas-phase flow through the bentonite to commence.

The proportion of the void volume above the breach is given by ε, and the time at which the water level in the canister falls below the breach is given by t_ε. Note that in general there are two times at which $V_g = \varepsilon V_v$; t_ε is the solution for which $p_a(t_\varepsilon) > p_b$).

At any time $t > t_\varepsilon$, in the period before which gas-phase flow commences, the pressure in the canister is given by (see equation 6.1.4)

$$p(t) = \frac{p_o(V_v + tg_o)}{\varepsilon V_v} = \frac{p_o}{\varepsilon}\left(1 + \frac{tg_o}{V_v}\right) . \qquad (6.1.10)$$

This is the equation of a straight line with intercept p_0/ε and gradient $(p_0 g_0/\varepsilon V_v)$.

6.2 Comparison with Earlier Results

In a previous study [4], a cylindrical crack was considered of width $2l$ running round the entire circumference of the canister; equations identical to equations (6.1.3) and (6.1.4) were derived for the period of water inflow and outflow, but with a different constant K_2^* given by

$$K_2^* = 2\pi^2 \frac{k}{\mu} \frac{r_c}{\log(b/l)} , \qquad (6.2.1)$$

where r_c is the radius of the canister, b is the thickness of bentonite, and l is the half-width of the breach. It should be noted that a typographical error in equation (A10) of [4] means that the π^2 term appears there simply as π; however the value of K_2^* used in those calculations contains the correct factor [21].

It can be argued (as in subsection 6.1) that, where the breach lies close to the edge of the canister, it is more appropriate to use a value of K_2^* that is increased by a factor of between 1 and 1.5, with the maximum value being taken when the breach is at the edge.

It is possible to reproduce exactly the mathematical problem solved in [4] by choosing an appropriate value of a in equation (6.1.2):

$$a = \frac{b\pi r_c}{b\log(b/l) + \pi r_c} \quad . \tag{6.2.2}$$

The parameter values used in [4] in comparing results with those in [20], together with the value of K_2^* used [21] are given in Table 3.

In that study [4], the ordinary differential equation was solved numerically, so a useful check on the correctness of the analytical solution is to compare the results obtained by the two methods for a corresponding set of parameter values. The results presented in Figures 24 and 25 of [4] have been used for this purpose. The results of [20] have been taken from Figure 8 of that report.

The results calculated for the volume of water in the canister and the corresponding pressure at any given time are shown in Figure 6. Four curves are plotted on each Figure, these curves corresponding to the following cases:

(i) solution obtained using equation (6.1.9) ($K_1^* = 1.80\ 10^{-17}\ m^{-3}s^{-1}Pa^{-1}$);
(ii) solution obtained using equation (6.1.9) ($K_1^* = 2.70\ 10^{-17}\ m^{-3}s^{-1}Pa^{-1}$);
(iii) results of [4] ($K_2^* = 1.80\ 10^{-17}\ m^{-3}s^{-1}Pa^{-1}$);
(iv) results of [20].

A comparison between the plots for cases (i) and (iii) shows an almost exact correspondence between the two sets of results; this is to be expected because they represent an analytical and a numerical solution of the identical mathematical problem with the same parameter values. This confirms the correctness of the analysis and calculations.

A comparison between the plots for cases (ii) and (iv) shows that increasing the values of K_1^* and K_2^* by a factor 1.5 (to take account of the modified geometry in the mathematical model in the case of a breach along the edge of the canister) gives an excellent match with the results of [20] during the inflow period, although there is some discrepancy at later times.

The previous study [4] concluded that the agreement between calculated results and those in [20] justified the use of a simplified model. The modification suggested in this paper (i.e. increasing the value of K_1^* and K_2^* by a factor 1.5 for a breach at the edge of the canister) has been shown to lead to even better agreement with the results during the inflow period in [20]. However, some discrepancy is observed during the outflow period, particularly in the calculated pressures.

In practice it is likely that uncertainties in the other parameters that influence K_1^* and K_2^* will result in an uncertainty of a factor of 1.5 in the value to be used being of little significance.

6.3 Results of Calculations

This study is concerned with the effects of a small breach at one point on the canister. Results are presented for four cases; the base case differs from the case in [4] in the following respects:

(i) base case: point breach with radius 2.5 10^{-3}m, void volume of 0.35 m^3 and a gas generation rate of 0.8 m^3(at STP)yr^{-1} (K_1^* = 1.58 10^{-19} $m^3s^{-1}Pa^{-1}$).

The remaining sensitivity cases are variations on the base case:

(ii) breach radius increased to 2.5 10^{-2}m (K_1^* = 1.69 10^{-18} $m^3s^{-1}Pa^{-1}$);

(iii) void volume increased to 1 m^3 (K_1^* = 1.58 10^{-19} $m^3s^{-1}Pa^{-1}$);

(iv) gas generation rate reduced to 0.08 m^3(at STP)yr^{-1} (K_1^* = 1.58 10^{-19} $m^3s^{-1}Pa^{-1}$).

The variations of water volume and canister pressure with time are shown in Figure 7 for these four cases.

The base-case results show that for a breach of this small size, and with the maximum gas generation rate, the amount of water entering the canister is extremely small (less than 3 10^{-4} m^3 in total) and the water flow occurs over a relatively short timescale (approximately 40 years).

An increase in the aperture by a factor of 10 results in an increase in the water flux by a factor of approximately 10, although this has no effect on the timescales of the water flow.

An increase in the void volume by a factor of approximately three results in an increase in the total water influx and an extension of the timescale by a factor of approximately three in each case.

A decrease in the gas generation rate by a factor of 10 results in an increase in the total water influx and an extension of the timescale by a factor of approximately 10 in each case.

The pressure plots can all be approximated by straight lines, which is to be expected since the water influx is so small; the gradient of these lines depends simply on the ratio of gas generation rate to void volume, and this is what is observed (noting that the pressure results from cases (i) and (ii) are indistinguishable). The pressure increases to approximately twice the hydrostatic pressure on the timescale during which water flows are taking place.

The most significant difference between these results and those in [4] is the very low water influx, which results from the combination of small breach size and high gas generation rate. A simple component mass balance was used to estimate the amount of water consumed by a corrosion reaction producing hydrogen at the maximum gas generation rate; this estimate was approximately 6 10^{-4} m^3yr^{-1}. The initial water influx rates estimated from the results in [4] for a circumferencial breach exceed this value by a factor of five. However, the initial water influx rates calculated here for a small circular breach (radius 2.5 mm) are a factor of 20 smaller than required and will certainly not be sufficient to support this reaction without some other source of water. The effects of this lower water influx on the gas generation rate may therefore need to be evaluated further.

7. LONG-TERM FATE OF THE GAS

Even at the maximum gas generation rate being considered (0.8 m^3(at STP)yr^{-1}) the calculations reported here show that once the gas escapes from the bentonite it will pass into the tunnel or damaged zone and then up towards the surface through the fracture network, with relatively little hindrance. A small amount of gas may remain trapped in the tunnel or in the damaged zone, but calculations have shown that a generous upper bound for this volume of trapped gas is only approximately 12 m^3(at STP). Over the long timescales considered in a repository performance assessment, any resulting delay in the migration of the gas is, in general, unlikely to be

significant. However, it should be noted that in the case of migration of H^3H, a delay in gas migration could be significant because of the short half-life of ^3H (approximately 12.3 years). The water flowing through the tunnel and damaged zones may be able to dissolve at most 25% of the gas; however, this estimate represents a maximum that could only be achieved if all the groundwater flowing in these zones was contacted by the gas, which was in turn dissolved up to the saturation concentration. In practice, the proportion of gas dissolved by the groundwater is expected to be considerably less than this. The gas will eventually pass into the rock overlying the repository. Two alternative approaches have been adopted to assess the ease with which the gas can pass upwards through the rock towards the surface; both the continuum model and the discrete fracture model results suggest that there is ample capacity to transport the gas away from the repository and up towards the surface. On the assumption that the confinement of the flow to channels lying along the intersections between fracture planes restricts the contact between the gas and the water, the regional groundwater flow is insufficient to dissolve more than a small fraction (some 5%) of this gas and so most of it will eventually reach the surface.

If the gas generation rates are lower than the maximum rate considered, a correspondingly greater proportion of the gas might be dissolved in the groundwater flow or trapped in the tunnel area. It should be noted that the estimates of these volumes of gas represent upper bounds that might be significant overestimates; if representative gas generation rates were reduced to 10% of the maximum value, it would be appropriate to try to obtain tighter bounds on these estimates.

8. CONCLUSIONS

The following set of conclusions can be drawn from this study:

(a) The long-term effect of hydrogen gas generation will depend on the gas generation rate and on the ability of the bentonite barrier to permit the escape of the gas.

(b) This study has considered a number of alternative gas migration routes through the bentonite including both the solution of gas in the groundwater and the flow of a gas phase. The amount of gas that could escape through the bentonite by dissolving in the groundwater and diffusing away from the canister is small compared with the maximum

gas generation rate that has been considered. Gas-phase flow through the bentonite must therefore represent the main route for the gas to escape. However, if the gas generation rate were significantly less than the maximum rate assumed in these calculations, the proportion of gas removed by dissolution and advection in groundwater would be correspondingly greater.

(c) The relationship between the pressure drop across the bentonite and the resulting gas-phase flow rate has been addressed both for a single capillary-like pathway with specified radius and for a large number of pathways with a specified distribution of radii. The scope of this analysis has been limited by the availability of experimental data relating to the mechanisms controlling gas-phase flow through water-saturated bentonite.

(d) Two crucial questions need to be addressed in the future with regard to the passage of gas through the bentonite and the degree of overpressurization of the canister. These questions relate to:

(i) The numbers (and size) of capillary-like pathways that are present in the bentonite. If the pathways present in the bentonite are sufficient in numbers and in size to permit gas-phase flow at the maximum generation rate without approaching the swelling pressure too closely, then the gas will be able to escape through the bentonite and make its way in due course to the surface.

(ii) The behaviour of the bentonite in response to increasing gas pressure, with respect to the enlargement of existing pathways and the formation of new pathways. If the pathways are insufficient, then it becomes important to consider the formation and enlargement of pathways by the displacement of clay aggregates. The effectiveness of this process will determine whether the gas can escape while avoiding any excessive increase in gas pressure in the canister that might compromise the integrity of the repository.

(e) Once the gas has escaped from the bentonite, it will pass into the tunnel area and the damaged zone. Gas-trapping in these zones could cause some delay in the passage of the gas to the surface, but is

unlikely to be significant over the long timescales that are considered in repository performance assessments. Solution of gas in the groundwater, and transport from these zones by diffusion or by advection in the groundwater flow, is unlikely to represent a significant transport pathway at the gas generation rates considered in this study. Clearly a reduction in the gas generation rates might affect the relative importance of the different gas migration pathways.

(f) The gas will eventually pass into the rock overlying the repository. Two alternative approaches have been adopted to assess the ease with which the gas can pass upwards through the rock towards the surface; both the continuum model and the discrete fracture model results suggest that there is ample capacity to transport the gas away from the repository and up towards the surface.

(g) The gas generation rate is dependent on the availability of water in the canister for the anaerobic corrosion of steel to take place. The model of water ingress into the canister suggests that for very small breach sizes the amount of water entering the canister may also be small; future studies should address what effect reduced water ingress might have on the gas generation rate. The amount of water that enters the canister and that is subsequently expelled is also important since it represents a potential radiological hazard, as a result of contamination of the water with ^{3}H while it is inside the canister.

REFERENCES

1. *Final Disposal of Spent Nuclear Fuel: Importance of the Bedrock for Safety*, SKB Technical Report 92-20, 1992.

2. P. Sellin, *Personal Communication*, 1993.

3. G.P. Marsh, *A Preliminary Assessment of the Advanced Cold Process Canister*, AEA Report AEA-InTec-0011, 1990.

4. J. Henshaw, A. Hoch and S.M. Sharland, *Further Assessment Studies of the Advanced Cold Process Canister*, AEA Report AEA-D&R-0060, 1990.

5. L. Börgesson, *Scenario of SKB/TVO-Canister with Special Respect to the Effect of Bentonite Intrusion into the Canister*, SKB Work Report AR 90-31, 1990.

6. L. Werme, *Near-field Performance of the Advanced Cold Process Canister*, SKB Technical Report 90-31, 1990.

7. R. Pusch, *Swelling Pressure of Highly Compacted Bentonite*, SKBF/KBS Technical Report 80-13, 1980.

8. R. Pusch, I. Neretnieks and P. Sellin, *Description of Transport Pathways in a KBS-3 Type Repository*, SKB Technical Report 91-49, 1991.

9. L. Romero, L. Moreno and I. Neretnieks, *A Compartment Model for Solute Transport in the Near Field of a Repository for Radioactive Waste (Calculations for Pu-239)*, SKB Technical Report 91-48, 1991.

10. I. Neretnieks, *Diffusivities of Some Dissolved Constituents in Compacted Wet Bentonite Clay-MX80 and the Impact on Radionuclide Migration in the Buffer*, SKBF/KBS Technical Report 82-27, 1982.

11. T.E. Eriksen and A. Jacobsson, *Diffusion of Hydrogen, Hydrogen Sulphide and Large Molecular Weight Anions in Bentonite*, SKBF/KBS Technical Report 82-17, 1982.

12. I. Neretnieks and C. Skagius, *Diffusivitetsmatningar av metan och vate i vat lera*, KBS TR-86, 1978.

13. W.R. Rodwell and P.J. Nash, *Mechanisms and Modelling of Gas Migration from Deep Radioactive Repositories*, UK Nirex Ltd Report NSS/R250, 1992.

14. H.S. Carslaw and J.C. Jaeger, *Conduction of Heat in Solids*, Second Edition, OUP, 1959.

15. R. Pusch, L. Ranhagen and K. Nilsson, *Gas Migration through MX-80 Bentonite*, Nagra Technical Report 85-36, 1985.

16. R. Pusch, *Behaviour of Hydrogen Gas in Deposition Holes and Its Dissipation through Confining Rock—Application to the KBS-3 Repository Design*, SKB Work Report AR 90-25, 1990.

17. R. Pusch and T. Fosberg, *Gas Migration through Bentonite Clay*, SKBF/KBS Technical Report 83-71, 1983.

18. M. Wiborgh, L.O. Höglund and K. Pers, *Gas Formation in a L/ILW Repository and Gas Transport in the Host Rock*, Nagra Technical Report 85-17, 1986.

19. L. Moreno and I. Neretnieks, *Gas, Water and Contaminant Transport from a Final Repository for Reactor Waste*, SKB Progress Report SFR 85-09, 1985.

20. L. Börgesson, *Some Aspects of the Water Intrusion Scenario for the Advanced Cold Process Canister*, SKB Work Report AR 90-12, 1990.

21. A. Hoch, *Personal Communication*, 1993.

TABLES

Table 1 Summary of Standard Data Values Used in This Study

Parameter	Value	Unit
Water viscosity	10^{-3}	Pa s
Water density	10^{3}	kg m^{-3}
Hydrogen gas viscosity	10^{-5}	Pa s
Depth of repository	500	m
Surface pressure	0.1	MPa
Hydrostatic pressure in repository	5.0	MPa
Henry's law constant for hydrogen (at 20°C)	0.166 10^{-6}	$m^3m^{-3}Pa^{-1}$
Surface tension of water	0.073	N m^{-1}

Table 2 Cross-sectional Area, Water Flux and Maximum Advection Rate of Dissolved Gas for Each Zone

Zone	Area (m^2)	Water flux ($m\ s^{-1}$)	Maximum advection rate of dissolved gas (m^3(at STP)yr^{-1})
Tunnel backfill	15.90	$3.0\ 10^{-12}$	$1.25\ 10^{-3}$
Blast-damaged	17.28	$3.0\ 10^{-10}$	$1.346\ 10^{-1}$
Stress-damaged	109.96	$3.0\ 10^{-11}$	$8.64\ 10^{-2}$
Total			**$2.223\ 10^{-1}$**

Table 3 Parameter Values Used in Previous Study of Gas-Water Interactions [4]

Parameter	Value	Unit
Void volume, V_v	1	m^3
Hydrostatic pressure in repository, p_b	5	MPa
Initial canister pressure, $p_a(0)$	0.1	MPa
Bentonite permeability, k	10^{-20}	m^2
Water viscosity, μ	10^{-3}	Pa s
External radius of canister, r_c	0.400	m
Thickness of bentonite, b	0.350	m
Width of circumferencial breach, $2l$	0.010	m
Half-width of breach, l	0.005	m
Derived constant, K_2^*	$1.80\ 10^{-17}$	$m^3s^{-1}Pa^{-1}$

FIGURES

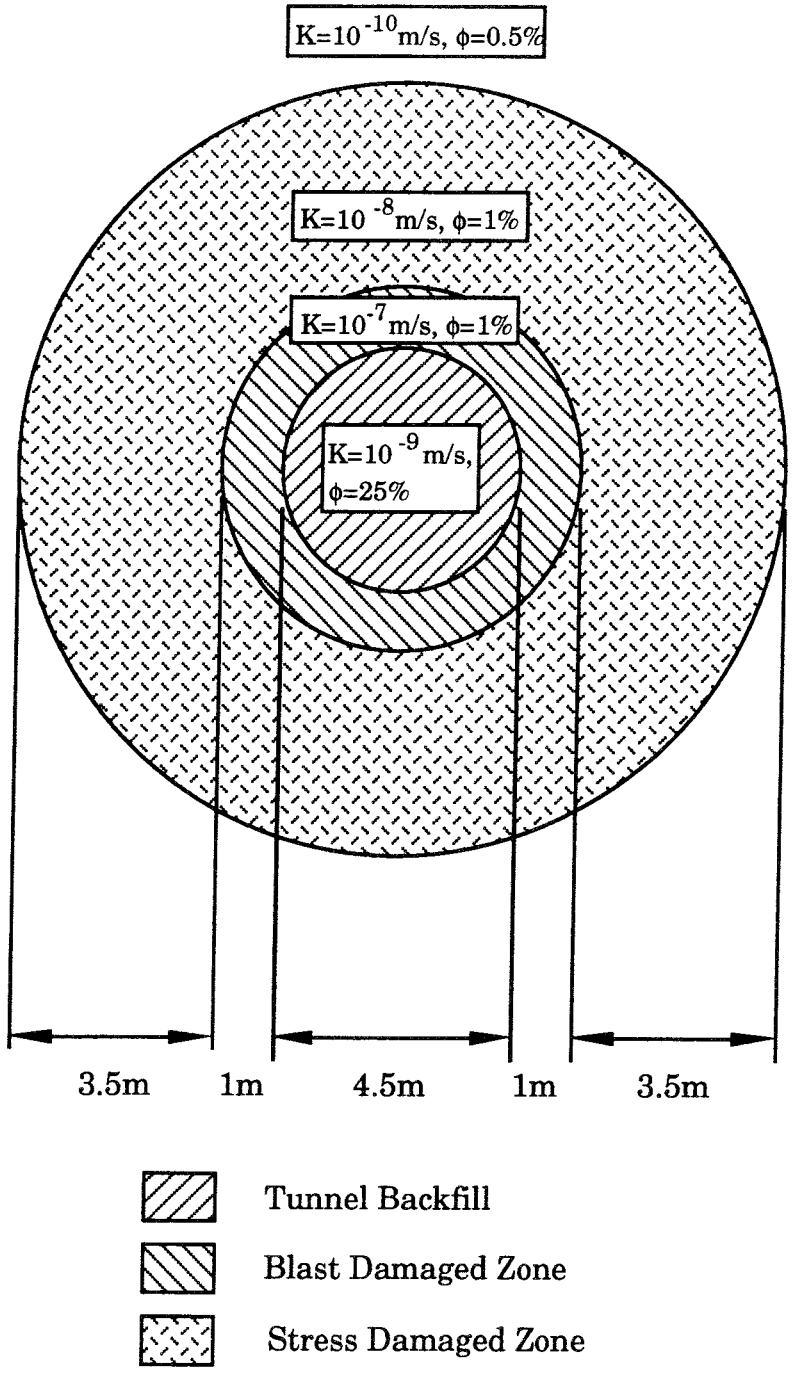

Figure 1 **Schematic cross section of the KBS-3 tunnel and damaged zones (hydraulic conductivities, *K*, correspond to the conservative case—see subsection 3.3).**

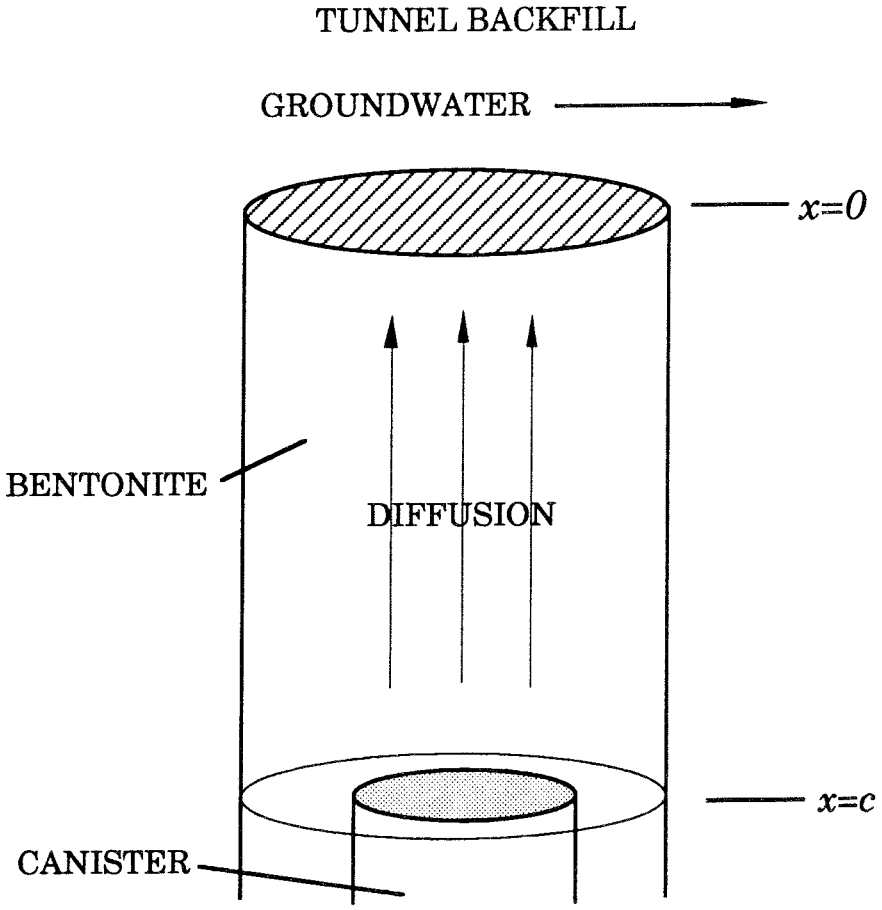

Figure 2 Schematic diagram of vertical diffusion in deposition hole.

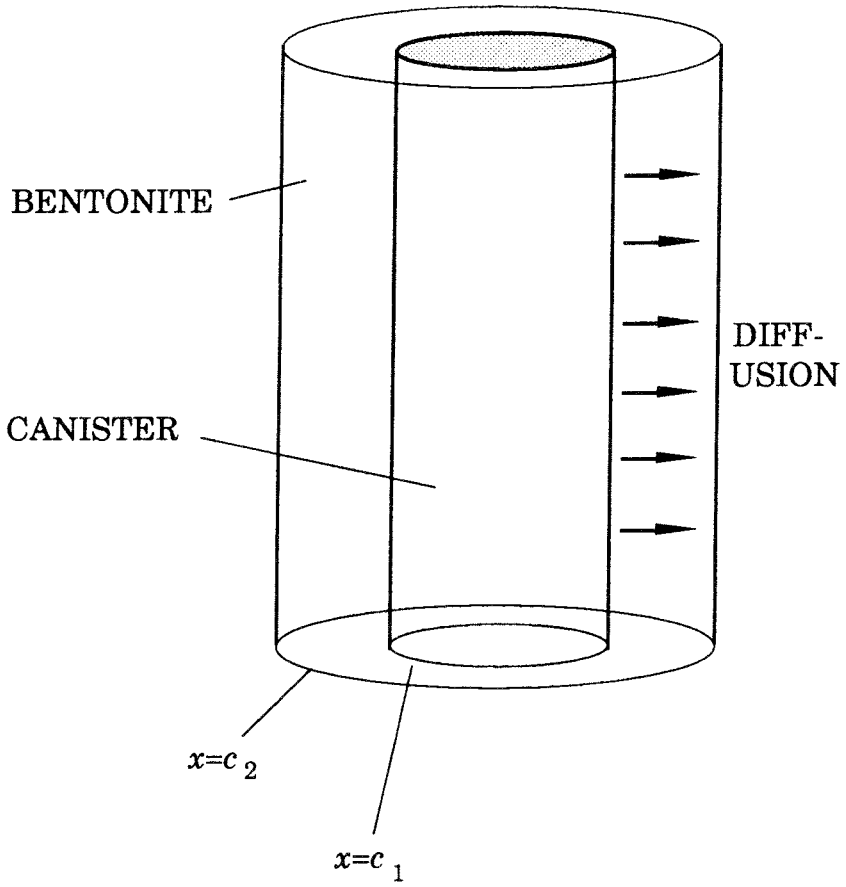

Figure 3 Schematic diagram of cylindrical diffusion in deposition hole.

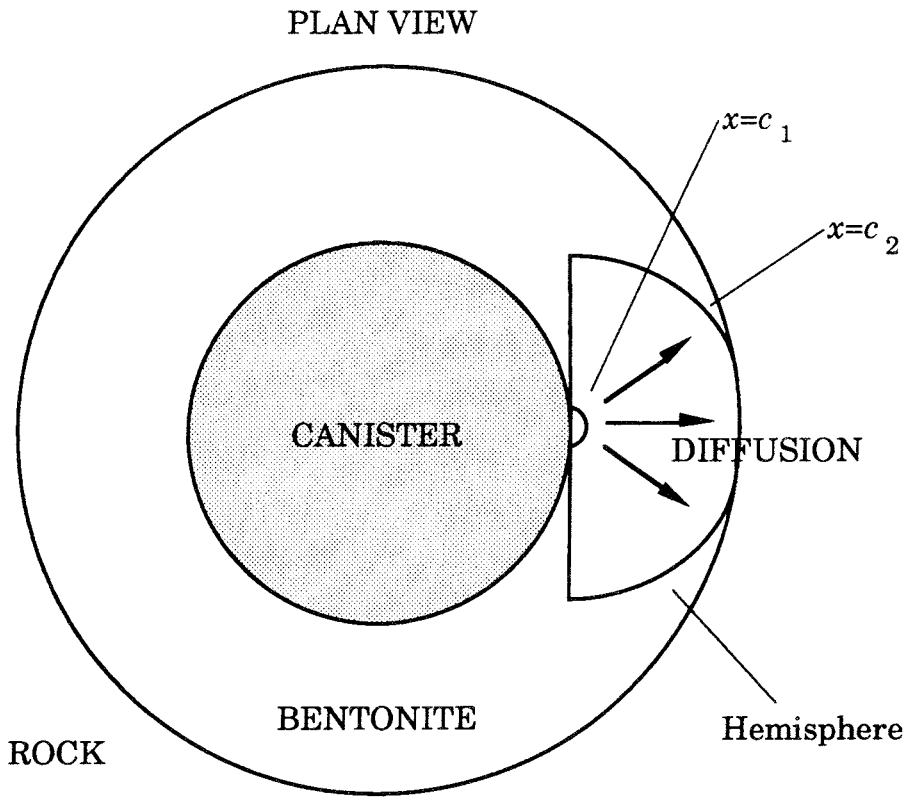

Figure 4 Schematic diagram of spherical diffusion in deposition hole.

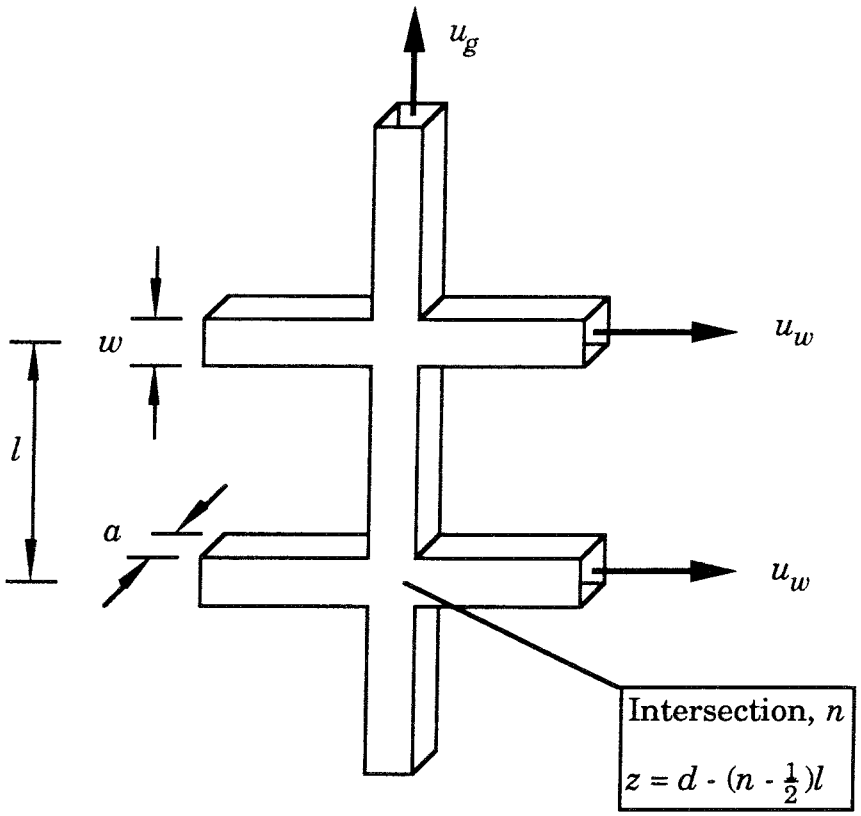

Figure 5 Schematic diagram of discrete advection model.

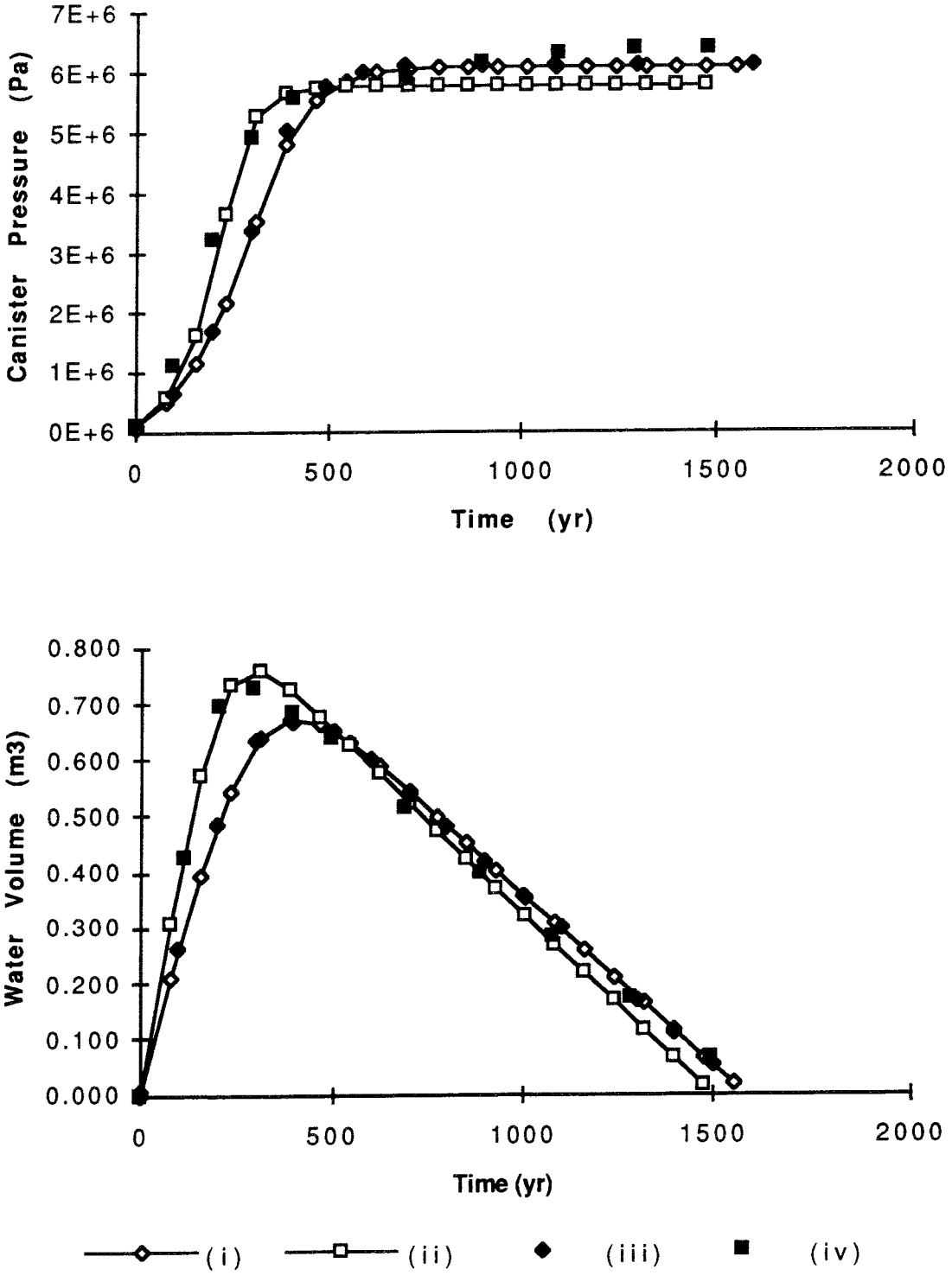

Figure 6 Evolution of canister pressure and water volume as a function of time: comparison of results obtained using analytical solution (cases (i) and (ii)) with previous studies of gas-water interactions (cases (iii) [4] and (iv) [20]).

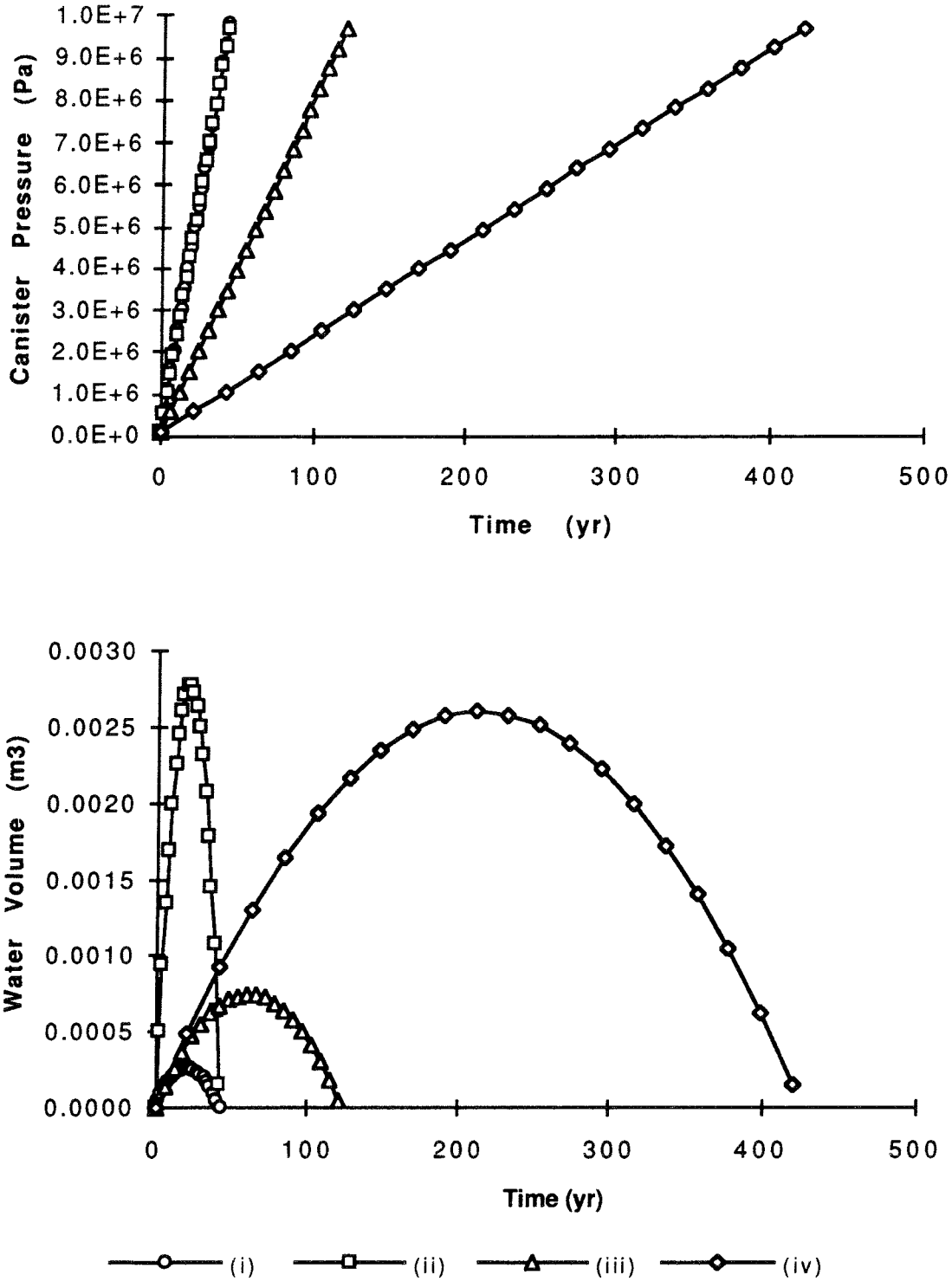

Figure 7 Evolution of canister pressure and water volume as a function of time: sensitivity of results obtained using analytical solution to variation of the parameters (see subsection 6.3).

APPENDIX A USE OF COMPUTER MODELLING TECHNIQUES FOR ESTIMATING GAS GENERATION RATES

The assessment of gas migration described in this report has been based on previous estimates of the hydrogen generation rate within the disposal canisters [A1–A3] (see subsection 3.1 above). Those estimates were derived by analytic techniques, various assumptions concerning the water ingress scenario and the geometry of the canisters. This Appendix describes a mathematical model and associated computer program, GAMMON, that have been developed under the Nirex Safety Assessment Research Programme to estimate gas generation rates from a variety of mechanisms, one of which is the anaerobic corrosion of carbon steel. This model could be used to confirm previous estimates of the hydrogen generation rate after failure of the canister, and to address some of the issues raised in the previous assessments. A description of the metal corrosion model is given in subsection A1, and the potential application of the model to hydrogen generation in the spent fuel disposal cansiters is discussed in subsection A2.

A1 Description of Modelling Approach

A mathematical model and associated computer program, GAMMON [A4], have been developed to model gas generation in radioactive waste repositories by the coupled processes of metal corrosion and microbial degradation of cellulosic wastes. In the application of GAMMON to the canisters, only hydrogen generation from anaerobic corrosion of carbon steel would be modelled. The model incorporates a set of chemical reactions that are representative of the likely metal corrosion reactions under the range of physical and chemical conditions that may exist in the respository.

Since iron is the major component of steel, it is the corrosion of iron that is assumed to be the major contributor to gas generation by this mechanism, and that is incorporated in the model. Because the canisters will initially contain trapped oxygen, corrosion is considered to proceed by means of a three-stage process encompassing both the aerobic and anaerobic regimes. The three representative reactions in the corrosion model are given in Figure A1.

The first stage involves the aerobic corrosion (or 'rusting') of iron metal. When sufficient of the oxygen has been used up such that the environment becomes essentially anaerobic, the mechanism enters the second stage in

which the oxide film is reduced to Fe_3O_4 ('magnetite'). In the second stage, magnetite is assumed to spall, thus exposing bare iron metal and allowing the third stage, that of anaerobic corrosion, to occur.

Two independent models are employed, both based on this chemical process, but exploiting the differences in geometry between plates and spheres. For any initial quantity of metal, plates and spheres represent the two extremes with regard to rate of loss of metal, and thus the two models cover the likely limits of gas generation. In the case of the canisters, this would allow differentiation of the steel shell and end caps, which could be modelled as plates and spheres respectively.

The metal corrosion rates within the repository are likely to be conditioned by the chemical environment. In the absence of chemical conditioning, the aerobic metal corrosion rate (i.e. the rate for the first stage of the mathematical model), R_1, for example, is given by

$$R_1 = \rho_1 \ , \tag{A1}$$

where ρ_1 is a constant metal corrosion rate that applies under optimal conditions. This corrosion rate is conditioned according to the chemical characteristics of the repository environment. For example,

$$R_1 = \rho_1 \frac{[O_2]}{[O_2] + K_s} \ , \tag{A2}$$

where $[O_2]$ is the concentration of oxygen and K_s is a constant saturation coefficient. If there is a significant concentration of oxygen in the system, the fraction $[O_2]/([O_2] + K_s)$ is approximately unity and the corrosion rate is not significantly altered. On the other hand, if the concentration of oxygen is low, that is the system is almost anaerobic, the fraction tends to zero and the aerobic metal corrosion rate is greatly reduced. The relationship between R_1 and ρ_1 in equation (A2) has been derived to represent this behaviour.

The anaerobic metal corrosion rate (i.e. the rate for the third stage of the mathematical model), R_3, is conversely given by

$$R_3 = \rho_3 \left[1 - \frac{[O_2]}{[O_2] + K_i} \right] \ , \tag{A3}$$

where ρ_3 is the anaerobic metal corrosion rate under optimal conditions and K_i is an inhibition coefficient. In this case, if there is a significant

concentration of oxygen in the system, the quantity $(1 - [O_2]/([O_2] + K_i))$ tends to zero and the anaerobic corrosion rate is greatly reduced. On the other hand, if the concentration of oxygen is low, the same quantity is approximately unity, and the anaerobic corrosion rate is not significantly altered from its optimal value. The values of K_s and K_i are determined by empirically fitting to observed data.

A2 Use of the Mathematical Model for Long-Term Corrosion Modelling

An important aspect of any assessment of post-closure repository performance is the estimation of gas generation rates over very long periods of time, and the GAMMON program can be used for this purpose. The program can be used to estimate gas generation rates in radioactive waste repositories (e.g. [A5]), or in individual waste packages. In the case of the canisters, the program could be used to confirm the analytic hydrogen generation rates and timescales estimated previously, and also to assess the sensitivity of the generation rate to variations in parameters such as the anaerobic corrosion rate of carbon steel and the degree of saturation of the canister. The latter issue was identified as one that may need to be addressed in future studies (see item (g) of Section 8 above).

As an example of how GAMMON could be applied to the canisters, time-varying hydrogen generation rates have been calculated for a steel canister of arbitrary dimensions using a range of anaerobic carbon steel corrosion rates. As suggested above, the canister shell was modelled as a plate and the end caps as spheres. For these illustrative calculations, the assumption was made that the canister was anaerobic and water saturated for the duration of the calculations. The calculated time-varying hydrogen generation rates are shown in Figure A2 for corrosion rates in the range 1 $\mu m\ yr^{-1}$ to 10 $\mu m\ yr^{-1}$, which is similar to the range given in subsection 3.1 above. The results illustrate the potential to estimate gas generation rates over the long timescales of interest in repository performance assessments. If required, different scenarios could potentially be modelled to address the issues mentioned above.

In addition, GAMMON could be applied to estimate the generation rate of H^3H resulting from contamination of the water with ^3H while it is inside the canister (see item (g) of Section 8 above).

References for Appendix A

A1. G.P. Marsh, *A Preliminary Assessment of the Advanced Cold Process Canister*, AEA Report AEA-InTec-0011, 1990.

A2. J. Henshaw, A. Hoch and S.M. Sharland, *Further assessment studies of the Advanced Cold Process Canister*, AEA Report AEA-D&R-0060, 1990.

A3. L. Werme, *Near-field Performance of the Advanced Cold Process Canister*, SKB Technical Report 90-31, 1990.

A4. G. Purdom and P.J. Agg, *GAMMON (Version 1A): A Computer Program Addressing Gas Generation in Radioactive Waste Repositories, Part A: Overview*, UK Nirex Ltd Report NSS/R338 (Part A), In preparation 1993.

A5. P.J. Agg, *Modelling Gas Generation in Radioactive Waste Repositories*, Nuclear Energy **32**(2), 81–87, 1993 (1992 Plowden Prize Paper (Under-30s Section)).

Figures for Appendix A

(a) *aerobic corrosion*

(i) $4Fe + 3O_2 \rightarrow 2Fe_2O_3$

(b) *oxide-film reduction*

(i) $4Fe_2O_3 + Fe \rightarrow 3Fe_3O_4$

(c) *anaerobic corrosion*

(i) $3Fe + 4H_2O \rightarrow Fe_3O_4 + 4H_2$

Figure A1 Chemical reactions in the metal corrosion model.

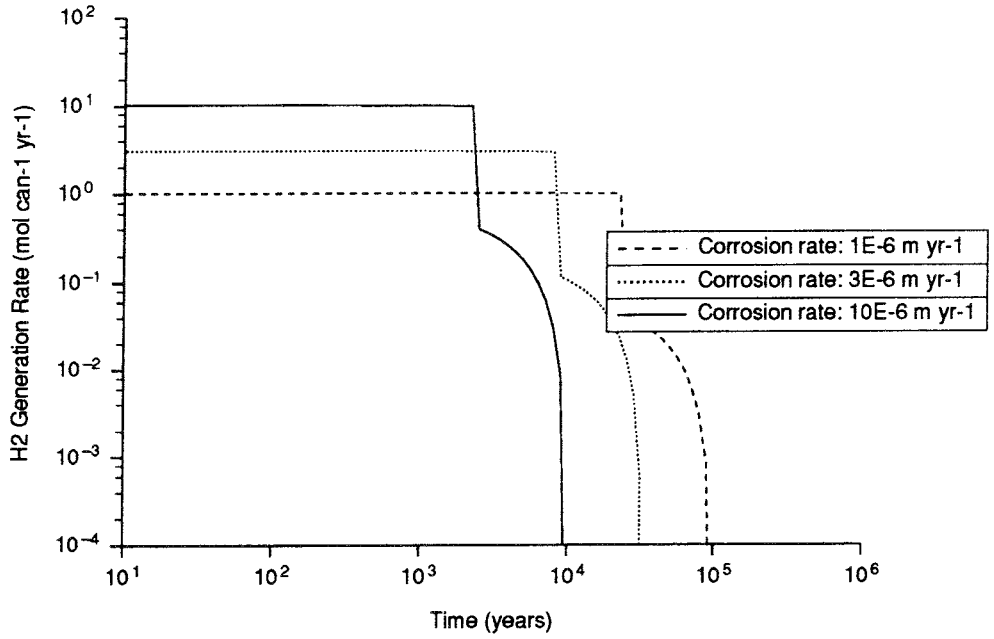

Figure A2 Hydrogen generation rate as a function of time in a hypothetical carbon steel disposal canister.

List of SKB reports

Annual Reports

1977-78
TR 121
KBS Technical Reports 1 – 120
Summaries
Stockholm, May 1979

1979
TR 79-28
The KBS Annual Report 1979
KBS Technical Reports 79-01 – 79-27
Summaries
Stockholm, March 1980

1980
TR 80-26
The KBS Annual Report 1980
KBS Technical Reports 80-01 – 80-25
Summaries
Stockholm, March 1981

1981
TR 81-17
The KBS Annual Report 1981
KBS Technical Reports 81-01 – 81-16
Summaries
Stockholm, April 1982

1982
TR 82-28
The KBS Annual Report 1982
KBS Technical Reports 82-01 – 82-27
Summaries
Stockholm, July 1983

1983
TR 83-77
The KBS Annual Report 1983
KBS Technical Reports 83-01 – 83-76
Summaries
Stockholm, June 1984

1984
TR 85-01
Annual Research and Development Report 1984
Including Summaries of Technical Reports Issued during 1984. (Technical Reports 84-01 – 84-19)
Stockholm, June 1985

1985
TR 85-20
Annual Research and Development Report 1985
Including Summaries of Technical Reports Issued during 1985. (Technical Reports 85-01 – 85-19)
Stockholm, May 1986

1986
TR 86-31
SKB Annual Report 1986
Including Summaries of Technical Reports Issued during 1986
Stockholm, May 1987

1987
TR 87-33
SKB Annual Report 1987
Including Summaries of Technical Reports Issued during 1987
Stockholm, May 1988

1988
TR 88-32
SKB Annual Report 1988
Including Summaries of Technical Reports Issued during 1988
Stockholm, May 1989

1989
TR 89-40
SKB Annual Report 1989
Including Summaries of Technical Reports Issued during 1989
Stockholm, May 1990

1990
TR 90-46
SKB Annual Report 1990
Including Summaries of Technical Reports Issued during 1990
Stockholm, May 1991

1991
TR 91-64
SKB Annual Report 1991
Including Summaries of Technical Reports Issued during 1991
Stockholm, April 1992

1992
TR 92-46
SKB Annual Report 1992
Including Summaries of Technical Reports Issued during 1992
Stockholm, May 1993

Technical Reports
List of SKB Technical Reports 1993

TR 93-01
Stress redistribution and void growth in butt-welded canisters for spent nuclear fuel
B L Josefson[1], L Karlsson[2], H-Å Häggblad[2]
[1] Division of Solid Mechanics, Chalmers University of Technology, Göteborg, Sweden
[2] Division of Computer Aided Design, Luleå University of Technology, Luleå, Sweden
February 1993

TR 93-02
Hydrothermal field test with French candidate clay embedding steel heater in the Stripa mine
R Pusch[1], O Karnland[1], A Lajudie[2], J Lechelle[2], A Bouchet[3]
[1] Clay Technology AB, Sweden
[2] CEA, France
[3] Etude Recherche Materiaux (ERM), France
December 1992

TR 93-03
MX 80 clay exposed to high temperatures and gamma radiation
R Pusch[1], O Karnland[1], A Lajudie[2], A Decarreau[3],
[1] Clay Technology AB, Sweden
[2] CEA, France
[3] Univ. de Poitiers, France
December 1992

TR 93-04
Project on Alternative Systems Study (PASS).
Final report
October 1992

TR 93-05
Studies of natural analogues and geological systems.
Their importance to performance assessment
Fredrik Brandberg[1], Bertil Grundfelt[1], Lars Olof Höglund[1], Fred Karlsson[2], Kristina Skagius[1], John Smellie[3]
[1] KEMAKTA Konsult AB
[2] SKB
[3] Conterra AB
April 1993

TR 93-06
Mineralogy, geochemistry and petrophysics of red coloured granite adjacent to fractures
Thomas Eliasson
Chalmers University of Technology and University of Göteborg, Department of Geology, Göteborg, Sweden
March 1993

TR 93-07
Modelling the redox front movement in a KBS-3 nuclear waste repository
L Romero, L Moreno, I Neretnieks
Department of Chemical Engineering,
Royal Institute of Technology, Stockholm, Sweden
May 1993

TR 93-08
Äspö Hard Rock Laboratory
Annual Report 1992
SKB
April 1993

TR 93-09
Verification of the geostatistical inference code INFERENS, Version 1.1, and demonstration using data from Finnsjön
Joel Geier
Golder Geosystem AB, Uppsala
June 1993

TR 93-10
Mechanisms and consequences of creep in the nearfield rock of a KBS-3 repository
Roland Pusch, Harald Hökmark
Clay Technology AB, Lund, Sweden
December 1992

TR 93-11
Post-glacial faulting in the Lansjärv area, Northern Sweden.
Comments from the expert group on a field visit at the Molberget post-glacial fault area, 1991
Roy Stanfors (ed.)[1], Lars O Ericsson (ed.)[2]
[1] R S Consulting AB
[2] SKB
May 1993

TR 93-12
Possible strategies for geoscientific classification for high-level waste repository site selection
Lars Rosén, Gunnar Gustafson
Department of Geology, Chalmers University of Technology and University of Göteborg
June 1993

TR 93-13
A review of the seismotectonics of Sweden
Robert Muir Wood
EQE International Ltd, Warrington, Cheshire, England
April 1993

TR 93-14
Simulation of the European ice sheet through the last glacial cycle and prediction of future glaciation
G S Boulton, A Payne
Department of Geology and Geophysics, Edinburgh University, Grant Institute, Edinburgh, United Kingdom
December 1992

TR 93-15
Analysis of the regional groundwater flow in the Finnsjön area
Anders Boghammar, Bertil Grundfelt, Hans Widén
Kemakta Konsult AB
June 1993

TR 93-16
Kinetic modelling of bentonite - canister interaction.
Implications for Cu, Fe, and Pb corrosion in a repository for spent nuclear fuel
Paul Wersin, Jordi Bruno, Kastriot Spahiu
MBT Tecnologia Ambiental, Cerdanyola, Spain
June 1993

TR 93-17
Oxidation of uraninite
Janusz Janeczek, Rodney C Ewing
Department of Earth & Planetary Science, University of New Mexico, Albuquerque, NM, USA
June 1993

TR 93-18
Solubility of the redox-sensitive radionuclides ^{99}Tc and ^{237}Np under reducing conditions in neutral to alkaline solutions. Effect of carbonate
Trygve E Eriksen[1], Pierre Ndalamba[1], Daqing Cui[1], Jordi Bruno[2], Marco Caceci[2], Kastriot Spahiu[2]
[1] Dept. of Nuclear Chemistry, Royal Institute of Technology, Stockholm, Sweden
[2] MBT Tecnologia Ambiental, Cerdanyola, Spain
September 1993

TR 93-19
Mechanical properties of fracture zones
Bengt Leijon
Conterra AB
May 1993

TR 93-20
The Fracture Zone Project - Final report
Peter Andersson (ed.)
Geosigma AB, Uppsala, Sweden
September 1993

TR 93-21
Development of "CHEMFRONTS", a coupled transport and geochemical program to handle reaction fronts
Catharina Bäverman
Department of Chemical Engineering, Royal Institute of Technology, Stockholm, Sweden
October 1993

TR 93-22
Carbon transformations in deep granitic groundwater by attached bacterial populations characterized with 16S-rRNA gene sequencing technique and scanning electron microscopy
Susanne Ekendahl, Johanna Arlinger, Fredrik Ståhl, Karsten Pedersen
Department of General and Marine Microbiology, University of Göteborg, Göteborg, Sweden
October 1993

TR 93-23
Accelerator transmutation of wastes (ATW)
– Prospects and safety
Waclaw Gudowski, Kjell Pettersson, Torbjörn Thedéen
Royal Institute of Technology, Stockholm, Sweden
November 1993

TR 93-24
Direct fault dating trials at the Äspö Hard Rock Laboratory
R H Maddock, E A Hailwood, E J Rhodes, R Muir Wood
October 1993

TR 93-25
Radially converging tracer test in a low-angle fracture zone at the Finnsjön site, central Sweden.
The Fracture Zone Project - Phase 3
Erik Gustafsson, Rune Nordqvist
Geosigma AB, Uppsala, Sweden
October 1993

TR 93-26
Dipole tracer experiment in a low-angle fracture zone at Finnsjön – results and interpretation.
The Fracture Zone Project – Phase 3
Peter Andersson, Rune Nordqvist, Tony Persson, Carl-Olof Eriksson, Erik Gustafsson, Thomas Ittner
Geosigma AB, Uppsala, Sweden
November 1993

TR 93-27

An approach to quality classification of deep groundwaters in Sweden and Finland

Marcus Laaksoharju[1], John Smellie[2],
Paula Routsalainen[3], Margit Snellman[4]
[1] GeoPoint AB, Stockholm, Sweden
[2] Conterra AB, Uppsala, Sweden
[3] Fintact Ky, Helsinki, Finland
[4] Imatran Voima Oy, Vantaa, Finland

November 1993

TR 93-28

Plan 93
Costs for management of the radioactive waste from nuclear power production

Swedish Nuclear Fuel and Waste Management Co

June 1993

TR 93-29

Diffusion of radionuclides in concrete/ bentonite systems

Y Albinsson[1], K Andersson[2], S Börjesson[1],
B Allard[3]
[1] Department of Nuclear Chemistry, Chalmers University of Technology, Göteborg
[2] Technical Environmental Planning, Chalmers University of Technology, Göteborg
[3] Department of Water in Environment and Society, University of Linköping

February 1993

TR 93-30

Core drilling by reverse flushing - a new drilling concept for small diameter boreholes

Christer Ljunggren
Vattenfall Hydropower AB

December 1993